

Substrate-induced conformational changes in the nucleotide-binding domains of lipid bilayer-associated P-glycoprotein during hydrolysis

Maria E. Zoghbi^{#1}, Leo Mok^{#2}, Douglas J. Swartz², Anukriti Singh², Gregory A. Fendley¹, Ina L. Urbatsch^{2,3} and Guillermo A. Altenberg^{1,3}

From the ¹Department of Cell Physiology and Molecular Biophysics, ²Department of Cell Biology and Biochemistry, and ³Center for Membrane Protein Research, Texas Tech University Health Sciences Center, Lubbock, Texas.

[#]These authors contributed equally to this work.

MEZ and GAF current address: School of Natural Sciences, University of California, Merced, 4225 N. Hospital Road, Atwater, California;

LM current address: Amgen Inc., Mail Stop ASF1-2101A, 1120 Veterans Blvd., South San Francisco, California;

DJS current address: Department of Natural Sciences, Lubbock Christian University, Lubbock, Texas,

Running title: *Conformations of Pgp in nanodiscs*

To whom correspondence should be addressed: Ina L. Urbatsch, Ph.D., Department of Cell Biology and Biochemistry, Texas Tech Health Sciences Center, 3601 4th Street, Lubbock, Texas 79430-6540. Telephone: (806) 743-2700 ext. 279; E-mail: ina.urbatsch@ttuhsc.edu; or Guillermo A. Altenberg, M.D., Ph.D., Department of Cell Physiology and Molecular Biophysics, Texas Tech Health Sciences Center, 3601 4th Street, Lubbock, Texas 79430-6551. Telephone: (806) 743-2531; FAX: (806) 743-1512; E-mail: g.altenberg@ttuhsc.edu

Keywords: ABC transporter; bilayer; FRET; LRET; luminescence resonance energy transfer; membrane; multidrug transporter; nanodiscs; spectroscopy

P-glycoprotein (Pgp) is an efflux pump important in multidrug resistance of cancer cells and in determining drug pharmacokinetics. Pgp is a prototype ATP-binding cassette (ABC) transporter with two nucleotide-binding domains (NBDs) that bind and hydrolyze ATP. Conformational changes at the NBDs (the Pgp engines) lead to changes across Pgp transmembrane domains that result in substrate translocation. According to current alternating access models (substrate binding pocket accessible only to one side of the membrane at a time) binding of ATP promotes NBD dimerization, resulting in external accessibility of the drug-binding site (outward-facing, closed NBD conformation), and ATP-hydrolysis leads to dissociation of the NBDs with the subsequent return of the accessibility of the binding site to the cytoplasmic side (inward-facing, open NBD conformation). However, previous work has not investigated these events under near-physiological conditions in a lipid

bilayer and in the presence of transport substrate. Here, we used luminescence resonance energy transfer (LRET) to measure the distances between the two Pgp NBDs. Pgp was labeled with LRET probes, reconstituted in lipid nanodiscs, and the distance between the NBDs was measured at 37°C. In the presence of verapamil, a substrate that activates ATP hydrolysis, the NBDs of Pgp reconstituted in nanodiscs were never far apart during the hydrolysis cycle, and we never observed the NBD-NBD distances of 10s of Å that have previously been reported. However, we found two main conformations that coexist in a dynamic equilibrium under all conditions studied. Our observations highlight the importance of performing studies of efflux pumps under near-physiological conditions, in a lipid bilayer, at 37°C, and during substrate-stimulated hydrolysis.

P-glycoprotein (Pgp, ABCB1, MDR1) exports hundreds of chemically unrelated, hydrophobic

compounds out of cells, including many therapeutic drugs (1). Pgp has been studied for over four decades for its involvement in multidrug resistance of cancer cells, and more recently for its importance in determining the pharmacokinetics of drugs used for treatment of HIV/AIDS, neurodegenerative and cardiovascular disorders (2,3). Because of its effects on pharmacokinetics the US Food and Drug Administration (FDA) mandates documentation of Pgp-drug interactions for approval of any new drug (4,5). An ongoing goal of the pharmaceutical industry has been the development of drugs that either selectively block Pgp or evade recognition by Pgp to achieve more favorable pharmacokinetics. Consequently, there is a great interest in understanding the mechanism by which drugs are transported by Pgp.

Pgp is a prototype ABC exporter that harnesses the energy from ATP binding and hydrolysis at the two nucleotide binding domains (NBDs) to power conformational changes in the transmembrane domains that lead to substrate translocation across the cell membrane. Pgp has been crystallized in nucleotide-free conformations with the NBDs ~30 Å apart, where a central cavity formed by the transmembrane helices is exposed to the inner leaflet of the membrane and the cytoplasm (Fig. 1, left) (6,7). More recent crystal structures of Pgp revealed even larger separation of the NBDs (8-10). Comparison of X-ray crystal structures of nucleotide-free and nucleotide-bound ABC transporters have led to the proposal of an alternating-access model where the central cavity is only accessible to one side of the membrane at a time (Fig. 1) (11). Despite decades of research the molecular mechanism of ABC transporters is still controversial. Data on different ABC transporters using diverse experimental methods such as Cys cross-linking (12,13), fluorescence (or Förster) resonance energy transfer (FRET) and luminescence (or lanthanide-based) resonance energy transfer (LRET) (14-18), double electron-electron paramagnetic resonance (DEER) spectroscopy (15,19-22), mass spectrometry (23), and electron microscopy (24-27), are not always in agreement. A number of models have been proposed as a result of experimental discrepancies, very limited number of structural studies under “physiological” conditions, and lack of high-resolution kinetic information. These models can be broadly divided into two categories,

monomer/dimer models (28-32), where ATP hydrolysis is followed by the complete dissociation of the NBDs, with NBD-NBD separations of tens of Å, and constant-contact models (33-36), where the NBDs remain in contact throughout the hydrolysis cycle, or remain in close proximity, and the power stroke results from smaller conformational changes at the NBD-NBD interface. In one constant-contact model, ATP hydrolysis is proposed to alternate between the two ATP binding sites, with the site that just performed the hydrolysis opening to allow ADP/ATP exchange in a partially opened NBD dimer (37,38). Independently on the extent of the conformational changes on the NBDs side, formation of a closed NBD dimer upon ATP binding seems to be coupled to rearrangements in the transmembrane helices that result in transition from an inward-facing conformation (Fig. 1, left; open conformation; dissociated NBDs or loosely-associated NBDs; binding pocket open to the membrane/cytoplasm) to an outward-facing conformation (Fig. 1, right; closed NBD dimer; dimeric NBDs; binding pocket open to extracellular side) from which the drug can dissociate into the external medium. Finally, hydrolysis of ATP promotes NBD dissociation, or dimer opening, resetting the pump for the next transport cycle.

Here, we used LRET to measure distance changes between the NBDs during the transport cycle of Pgp reconstituted in lipid nanodiscs (NDSCs). NDSCs are nm-scale discoidal structures that contain a phospholipid bilayer encased by membrane scaffold proteins (MSPs), which are soluble and stable (39). Although NDSCs differ from native membranes in physical properties such as curvature, and in the complexity of lipid composition, they are excellent lipid-bilayer platforms for spectroscopy and other applications. LRET is a highly sensitive spectroscopic technique that allows the study of proteins while they are functional in a native-like membrane environment and at physiological temperature (40-44). LRET, like the traditional FRET, is based on energy transfer from a donor to an acceptor, but in LRET a lanthanide (Tb^{3+} or Eu^{3+}) is used as donor. The use of luminescent lanthanides as donors has advantages for membrane protein studies over the traditional fluorescent donors used for FRET. Tb^{3+} displays

sharp atomic-like emission peaks with dark regions between the peaks that allow for measurements of the sensitized acceptor emission (due to resonance energy transfer) without contamination from the donor emission. Also, the long emission lifetime of the Tb^{3+} excited state (ms vs. ns of traditional fluorophores) makes delayed (gated) acquisition possible (generally acquisition is delayed 60-200 μ s from the excitation pulse). Gated acquisition minimizes the light scattering effects of structures such as detergent micelles, liposomes and NDSCs, and results in minimal background with high signal-to-noise ratio. Another major advantage is that the long lifetime sensitized acceptor emission makes the calculation of donor/acceptor distances independent of labeling stoichiometry because long lifetime emission from acceptors with intrinsic lifetimes in the ns range can only arise from energy transfer (44). We have recently shown the usefulness of our approach to study the NBD dimerization/dissociation process during the ATP hydrolysis cycle of the bacterial Pgp homolog MsbA (40,45). For the studies presented here, we introduced two Cys in a fully functional Cys-less Pgp (CL Pgp), at positions equivalent to those that we have used to characterize NBD movements in MsbA. The LRET probes (donor and acceptor) were chemically attached to these Cys and alterations in the distance that separates the probes were assessed from the changes in the sensitized-emission lifetimes. We show conformational changes on the Pgp cytoplasmic side in response to binding of the transport substrate in the transmembrane domain, and a degree of NBD dissociation much wider for Pgp in detergent than for Pgp reconstituted into lipid bilayers. Our data stresses the importance of performing structural studies of ABC exporters in a lipid bilayer and at physiological temperature.

Results

Characterization of the N606C/T1252C Pgp (NT Pgp)-Starting with a fully-functional CL Pgp, we introduced two Cys in positions equivalent to those that we used to study MsbA (18,40). To generate NT Pgp we started with our improved CL Pgp engineered by directed-evolution mutagenesis (46). In contrast to a previous all Cys-to-Ala variant [39,40], this CL Pgp is fully capable of drug transport. In NT Pgp, residues N607 and

T1252 of CL Pgp, near the carboxyl ends of each NBD, were substituted with Cys. These Cys are readily accessible to the aqueous environment for efficient labeling (6,8,10), and major changes in the distance between the Cys607-Cys1252 are expected between the inward-facing (closed NBD dimer) (38,47) and outward-facing (open NBDs) conformations (at least 30 Å; Fig. 1) (6-10). The NT Pgp mutant displayed wild-type-like drug resistance *in vivo*, indicating that it was capable of exporting drugs across the plasma membrane (Fig. 2A). Purified WT Pgp, CL Pgp and NT Pgp were >95% pure (Supplementary Fig. 1) and displayed robust Ver-stimulated ATPase activity in detergent-lipid micelles: 3.9 ± 0.4 , 3.5 ± 0.3 and 4.0 ± 0.5 μ mol/min/mg, respectively (n = 3 or more different preparations each) (48). In 2 experiments, the Ver-stimulated ATPase activity of the catalytically-inactive mutant NT/AA Pgp (NT Pgp with substitution of the catalytic carboxylates E552 and E1197 with A) was undetectable. Also, labeling with the LRET probes did not affect the ATPase activity of NT Pgp in NDSCs. The activities in the presence of 30 μ M verapamil (Ver) were 4.1 ± 0.24 and 4.1 ± 0.21 μ mol/min/mg for the labeled (n = 3) and unlabeled (n = 5) NT Pgp, respectively.

A typical size-exclusion chromatography elution profile of NT Pgp reconstituted in NDSCs is shown in Fig. 2B (black trace). The two main peaks correspond to NT Pgp in nanodiscs (left) and empty NDSCs (right). For most LRET experiments we used the fraction enriched in NT Pgp-NDSCs, but we also used affinity-purified NT Pgp in NDSCs (red trace); the results obtained without and with this additional extra purification step were essentially identical. Fig. 2C shows a Coomassie blue-stained (CB) PAGE-SDS of the fraction enriched in NT Pgp NDSC and a fluorescence image (Fluo) of the gel that confirms the specific labeling of NT Pgp by Bodipy FL. Fig. 2D shows that the dependence of Ver-stimulated ATP hydrolysis of NT Pgp-NDSCs and WT-Pgp in detergent-lipid micelles on [MgATP] was undistinguishable. However, the affinity for Ver was higher in the NDSCs (Supplementary Fig. 2). The ATPase activity of WT Pgp and NT Pgp in detergent-lipid micelles or NDSCs was stable for several h at 37°C, whereas Pgp ATPase activity at 37°C in detergent without lipids had a half-time

($t_{1/2}$) < 5 min (Supplementary Fig. 3). NT Pgp-NDSCs could be stored at 4°C for up to a week with little loss of activity. Overall, these results demonstrate that NT Pgp is active *in vivo* and *in vitro*.

Conformational changes of the NBDs during the ATP hydrolysis cycle of Pgp in nanodiscs—We chose the Tb³⁺-chelate/Bodipy FL donor/acceptor pair (Forster distance of 41 Å) to label the two Cys of NT Pgp to maximize sensitivity to the conformational changes predicted. This LRET donor/acceptor pair is highly-sensitive to distance changes in the ~30- to 55-Å range (Supplementary Fig. 4). NDSCs containing 0.5-1.0 μM of labeled NT Pgp were analyzed in a 3-mm pathlength cuvette at 37°C. NT Pgp-NDSCs labeled only with donor (Fig. 3A, black dashed trace, Tb only) showed typical Tb³⁺ emission peaks centered about 490 and 545 nm. NT Pgp-NDSCs labeled with donor and acceptor showed an additional peak around 515 nm that corresponds to the sensitized Bodipy FL emission that arises from LRET from Tb³⁺ (Fig 3A, solid lines). The intensity of this energy transfer is strongly dependent on the donor/acceptor distance and it is, therefore, a sensitive indicator of conformational changes. Addition of 5 mM NaATP produced a large increase of the LRET intensity (Fig. 3A, blue) compared to the intensity in the apo state (Fig. 3A, black; nucleotide and drug free). The EC₅₀ for ATP estimated from similar LRET experiments was 0.26 ± 0.06 mM (n = 5); thus, 5 mM ATP is a saturating concentration. Subsequent addition of MgSO₄ to start ATP hydrolysis caused a partial reversion (Fig. 3A, orange) towards the LRET intensity in the apo state (Fig. 3A, black). Subsequent addition of sodium orthovanadate (Vi; Fig. 3A, green), an inhibitor of Pgp ATPase activity that promotes the formation of a stable post-hydrolysis transition state (49), produced the strongest LRET intensity. A similar experiment performed with the catalytically inactive NT/AA Pgp (Fig. 3B) showed increased LRET intensity with the transition from the apo state to the ATP-bound state (black to blue), whereas MgSO₄ did not decrease LRET (orange) as in the active Pgp. This observation strongly suggests that the transition from the ATP-bound state to the MgATP state in Fig. 3A (blue to orange) was dependent on ATP hydrolysis. Together, these results show that LRET can be used to follow the

conformational changes of Pgp in NDSCs during the ATP-hydrolysis cycle.

A time course of the changes in LRET intensity is shown in Fig. 3C. The increase in intensity in response to the addition of NaATP (transition from apo state to ATP-bound state) was slow ($t_{1/2}$ ~20 s). This is likely due to the fact that MgATP, and not NaATP, is the true substrate for binding to the NBDs. We have presented evidence of a much faster rate of dimerization of isolated NBDs in response to MgATP (*vs.* NaATP) that might result from more favorable electrostatics for MgATP at the dimer interface (42). As expected, the changes in LRET intensities elicited by transitions to the MgATP and Vi states were much faster, and their kinetics could not be resolved in these manual mixing experiments.

The changes in LRET intensities described above can result from: 1) changes in donor/acceptor distances (higher LRET intensity results from shorter distances; *e.g.*, dimerizing NBDs), 2) changes in the proportion of molecules with dimeric *vs.* dissociated NBDs, or 3) a combination of both. To discriminate between these possibilities we assessed donor/acceptor distances and the distribution of donor-acceptor pair distances in different states. Fig. 3D shows typical LRET decays from NT Pgp-NDSCs under different experimental conditions. As expected from the results in Fig. 3A, the transition from the apo state to the ATP-bound state increased the Bodipy FL sensitized emission intensity (see early part of the Fig. 3D, blue *vs.* black) and accelerated the overall rate of decay. The latter is clearly evident in the semi-log plot (Fig. 3D inset). During continuous ATP hydrolysis (MgATP state; Fig. 3D, orange) the initial intensity and the decay rate were intermediate between those in the apo and ATP-bound states. In the semi-log plot inset (Fig. 3D) it is clear that the decays do not follow a single-exponential function, in which case they would appear as straight lines. The decays can be well fitted using a three-exponential decay function. As mentioned under Materials and methods, the fastest component is very small and is largely the result of the instrument response time. Therefore, there were only two dominant donor/acceptor distances under all the experimental conditions studied. These distances and the proportion of donor/acceptor pairs displaying each of the distances are summarized in

Table 1. The data revealed the coexistence of these two dominant conformations during the ATP hydrolysis cycle: 1) a short distance (d_1) where the LRET probes are separated by ~ 33 Å; d_1 is likely to correspond to the closely-associated NBD dimer conformation (Fig. 1, right); and 2) a longer distance (d_2) where the probes are separated by ~ 47 Å ($\Delta_{d_2-d_1} \sim 15$ Å); d_2 is likely to correspond to a conformation with dissociated NBDs. These two distances remained essentially unchanged in the apo, ATP-bound and MgATP states. The data in Table 1 indicated that the observed changes in the LRET intensities and decays illustrated in Fig. 3 were mainly the result of changes in the proportion of Pgp molecules in each of the two conformations. This behavior was similar to that previously described for MsbA (40,45). From the apo state to the ATP-bound state the % of molecules that adopted the closed NBD conformation d_1 increased from only ~ 10 to $\sim 40\%$. Transition from the ATP-bound state to the MgATP state decreased that number to $\sim 30\%$, as expected for a dynamic equilibrium between associating and dissociating NBDs during steady-state ATP hydrolysis (42,50). These results suggest that the open conformation of the Pgp NBDs is favored even under maximal ATPase activity. This is in agreement with electron microscopy studies (27,51). In summary, our data suggest that: 1) the NBDs of NT Pgp in NDSCs are more frequently dissociated during basal ATP hydrolysis, and 2) even though the NBD-NBD distance is much shorter than that expected from the Pgp crystal structures in detergent, the NBDs dissociate, supporting a monomer-dimer mode of operation.

It is important to note that the shorter separation between the NBDs in our studies is not the result of confining the protein in the NDSCs (~ 110 -Å diameter), because it was also observed in MsbA reconstituted in unilamellar liposomes of $\sim 1,000$ -Å diameter (18). Therefore, an important finding of the present study is that reconstitution of Pgp in a lipid bilayer constrains its conformations, and results in a more compact protein, in agreement with previous finding on MsbA (18). It is also important to stress that the standard deviations below 1 Å (Table 1) do not represent the error in the calculated vs. “real” distances, but are the result of the very high

experimental reproducibility of LRET with atomic resolution. There is an error when the donor/acceptor distance is assumed to correspond to the distance between the reacted thiols in the Cys side chains (unavoidable uncertainty about the position of probes due to their length). However, measurements by others and us have shown donor/acceptor LRET distances very close to those expected from crystal structures (40,42-44). Even though the size of the optical probes can introduce errors in the donor-acceptor vs. Cys side chains absolute distances, LRET, as FRET, is an excellent method to determine distance changes. Considering the free mobility of the optical probes in LRET and that we positioned them outside the active NBD interface, in a region that does not experience conformational changes during the nucleotide binding/hydrolysis cycle, LRET seems more than adequate to address domain movements in Pgp, and seems a good indicator of the changes in distance under different conditions. In any case, the important point is that the maximal difference between states can be as small as ~ 10 Å (see below).

Conformational changes in the NBDs during Pgp activation by verapamil-The ATPase activity of Pgp in lipid micelles or NDSCs is stimulated 5- to 10-fold by Ver (Supplementary Fig. 2). It has been proposed that the ATPase activity is stimulated because binding of transport substrate in the transmembrane region causes conformational changes that are transmitted to the NBDs, promoting their dimerization (52,53). Here, we tested this possibility with studies of the NBD-NBD interactions in NT Pgp reconstituted in NDSCs. Fig. 4A shows typical emission spectra of donor/acceptor-labeled NT Pgp in NDSCs under experimental conditions similar to those in Fig. 3A, but in the Ver-bound state ($30 \mu\text{M}$ Ver added to the NT Pgp in the apo state). Transition from the apo state (Fig. 4A, black) to the Ver-bound state (Fig. 4A, red) increased the LRET intensity, but subsequent addition of NaATP had little effect (Fig. 4A, blue, Ver/ATP-bound). This is in contrast to the clear increase observed in the transition from the apo state to the ATP-bound state in the absence of Ver (Fig. 3A, black vs. blue). Transition to the MgATP state in the presence of Ver increased LRET intensity (Fig. 4A, orange, Ver/MgATP), in marked contrast to the Mg-induced decrease in LRET intensity in the

absence of Ver (Fig. 3A, orange vs. blue). The effect of Ver was also observed in experiments performed in reversed order, where addition of Ver to NT Pgp-NDSCs actively hydrolyzing MgATP increased the LRET intensity to a value similar to that in the Ver/MgATP state in Fig. 4A (Supplementary Fig. 5). The effect of Ver on Pgp was fast, as can be seen in the time course of the LRET intensity changes in Fig. 4B. Transition from the Ver-bound state to the Ver/ATP-bound state produced little change in intensity, whereas transition to the Ver/MgATP state after addition of MgSO₄ produced a rapid increase in intensity, to a level close to the maximum reached after inhibition of ATP hydrolysis by Vi (Vi state). Again, the increase in LRET with the transition from the Ver/ATP-bound state to the state during continuous ATP hydrolysis (Ver/MgATP) is in clear contrast with the decrease in LRET intensity when hydrolysis starts in the absence of Ver (Fig. 3C).

The LRET decays showed higher intensities and faster decays for the Ver-bound (Fig. 4C, red) and Ver/ATP-bound (Fig. 4C, blue) NT Pgp-NDSCs compared to the apo state (Fig. 4C, black), and the intensity and speed of decay increased further in the Ver/MgATP state (Fig. 4C, orange). The analysis of the data (Table 1) indicates that the increase in LRET intensity in the presence of Ver was the result of a combination of two changes: shortening of the longer distance d2 by $2.2 \pm 0.3 \text{ \AA}$ ($P < 0.003$) and increase in the % molecules displaying closed NBD dimers (d1) by $5 \pm 1 \%$ ($P < 0.003$). The distance d2 in the Ver-bound state ($\sim 44 \text{ \AA}$) was maintained in the Ver/ATP, Ver/MgATP and Ver/Vi states, and might represent a semi-open conformation similar to that in the Vi state in the absence of Ver (Table 1).

Unexpectedly, transition from the Ver-bound state to the Ver/ATP-bound state had only a small effect on % of molecules with closed NBD dimers (Table 1 and Fig. 5A). However, the % of molecules displaying the distance d1 did increase in Ver/MgATP state to $\sim 40\%$ (Table 1 and Fig. 5A). This result is in marked contrast with the results in the absence of Ver, where the transition from the ATP-bound to the MgATP state was accompanied by a decrease in the % of molecules with donor/acceptor pairs showing distance d1 (Table 1 and Fig. 5A). Hence, ATP hydrolysis

induced by addition of Mg²⁺ results in different conformational changes in the ATP-bound state (absence of transport substrate) and Ver/ATP-bound state (basal vs. Ver-stimulated hydrolysis). In summary, under steady-state ATP hydrolysis Ver promoted the formation of the closed NBD dimer conformation (~ 40 vs. $\sim 30\%$ of the molecules) and reduced the separation between the NBDs in the open conformation (Table 1 and Fig. 5A).

Distribution of Pgp conformations during the hydrolysis cycle-Fig. 5B shows the average distribution of distances calculated from the LRET sensitized emission decays of NT Pgp NDSC in the presence of Ver using an exponential series method (see Materials and methods). Equivalent data in the absence of Ver can be found in Supplementary Fig. 6). The exponential series method analysis can recover lifetime distributions (which can be converted to distance distributions) without assumptions about the distributions shapes, and it can therefore be used to discriminate between discrete and continuous distributions (18,54,55). Clear peaks centered at distances that approximate d1 and d2 obtained from the multi-exponential fits (Table 1) confirmed the presence of two discrete conformations in NT Pgp-NDSCs under all experimental conditions studied (Fig. 5B): the first peak corresponding to the “closed NBD” conformation d1, and the second peak to the “open NBDs” conformation d2. The analysis suggests the predominance of well-defined conformations of Pgp as opposed to a broad distribution of conformations.

Fig. 5B also illustrates the shift of the d2 conformation peak towards shorter distances in the presence of Ver (Fig. 5C), as suggested by the discrete multi-exponential fittings discussed above. Particularly interesting is the observation that NT Pgp in NDSCs is more compact during hydrolysis in the presence of Ver (compare black and orange traces in Fig. 5D); 90% of the d2 Ver/MgATP molecules were within $\sim 7 \text{ \AA}$ ($42\text{-}49 \text{ \AA}$) whereas only 65% were in the absence of Ver.

Effects of temperature-The ATPase activity of Pgp is highly-sensitive to temperature (56). Here, we focused on the conformational changes of NT Pgp in NDSCs at 20°C. Fig. 6A shows representative emission spectra of NT Pgp-NDSCs where it is clear that the LRET intensity at 515 nm was lower than at 37°C (compare with Fig. 3A and

Fig. 4A). The calculated distances d_1 and d_2 in the apo state at 20°C were similar to those determined at 37°C (32.6 ± 0.8 and 48.7 ± 3.1 Å, respectively; $n = 3$). Very different from NT Pgp in NDSCs at 37°C (Fig. 3A), the responses to addition of ATP and MgSO₄ at 20°C were absent, although incubation with Vi for ~10 min produced a significant increase in the LRET intensity (Fig. 6A, green). Since Vi trapping of Pgp requires NBD dimerization and MgATP hydrolysis, the slow increase in LRET intensity coincides with the lower basal ATPase rate of Pgp at 20°C vs. 37°C (56). These results indicate that even in a lipid bilayer, at lower temperatures in the absence of substrate Pgp does not experience significant conformational changes during the catalytic cycle. The emission spectra in Fig. 6B illustrate the effect of Ver on NT Pgp-NDSCs at 20°C. Similar to the effect at 37°C (Fig. 4A), there was an increase in LRET intensity with the transition from the apo (Fig. 6B, black) to the Ver-bound state (Fig. 6B, red). Also similar to the responses at 37°C, the LRET intensity remained essentially unchanged after addition of ATP (Fig. 6B, blue; Ver/ATP-bound state), but increased significantly in the Ver/MgATP state (Fig. 6B, orange), and even more in the Vi state (Fig. 6B, green). The steady-state increase in LRET intensity was reached rapidly, consistent with the relatively high Ver-stimulated ATPase activity of NT Pgp-NDSCs at 25°C (1.6 ± 0.1 μmol/min/mg). The changes observed for the Ver-bound NT Pgp-NDSCs at 20°C and 37°C were similar, although the average % of molecules displaying the shorter distance d_1 was consistently lower at 20°C (apo state: $10 \pm 2\%$; Ver-bound state: $12 \pm 1\%$; Ver/ATP-bound state: $12 \pm 1\%$; Ver/MgATP state: $27 \pm 3\%$; Ver/Vi state: $37 \pm 5\%$; $n = 3$; compare with Table 1). The similar effect of Ver at 20°C and 37°C is consistent with the high degree of ATPase stimulation observed at both temperatures (5-fold and 7-fold, respectively). These results suggest that, although less efficiently than at physiological temperature, at 20°C Ver activates the ATPase activity of Pgp in NDSCs and also shifts the dynamic equilibrium towards the closed NBD dimer conformation.

Conformational changes of Pgp in nanodiscs vs. detergent—Here, we studied the conformational changes of Pgp in detergent at 20°C. Although Ver was present, the LRET decay curves in the apo,

Ver-bound, Ver/ATP-bound and Ver/MgATP states were indistinguishable (Fig. 6C, black, red, blue and orange, superimposed lower records), and only changed after incubation with Vi for several min (Fig. 6C, green; recorded after 20-min incubation with Vi). For comparison, the LRET intensity at 20°C in the Ver/MgATP state of NT Pgp-NDSCs was much larger (Fig. 6C, gray). These results indicate that the effect of Ver on Pgp conformation requires the presence of lipids, as has been previously suggested (57). Analysis of the LRET decays of NT Pgp in detergent at 20°C pointed to two coexisting conformations with a short distance of ~33 Å and a long distance of ~56 Å. The first distance is similar to those for NT Pgp-NDSCs at 20°C and 37°C; this is not surprising because it corresponds to the closed NBD dimer. The longer distance, however, was significantly longer than that calculated for NT Pgp in NDSCs at the same temperature. This is in agreement with our previous findings of a more compact conformation for MsbA in a lipid bilayer than in detergent (45). The longer average distance for NT Pgp in detergent is likely to underestimate the actual value because the calculated distance of ~56 Å is ~15 Å away from the Tb³⁺/Bodipy FL Förster distance, with $E \sim 0.15$ (see Supplementary Fig. 4). The difference between NT Pgp in detergent and nanodiscs is clearly illustrated by the d_2 distance distributions in Fig. 6D.

The importance of lipids to make Pgp more compact was also apparent in experiments where we added *E. coli* lipids to NT Pgp in detergent at 20°C in the apo state. In these experiments the low-intensity, slow decay measured in NT Pgp in detergent (Fig. 6C, black) was gradually replaced with faster decays as the amount of lipids increased (Supplementary Fig. 7). Analysis of the LRET sensitized-emission decays suggested that the effect of lipid addition was mostly the result of a decrease in the longer donor/acceptor distance. This suggests that the lipids help stabilize and activate Pgp by promoting NBDs association even in the presence of detergent. Significant light scattering prevented detailed studies of the conformational changes under different conditions, which points to the limitation of mixed detergent/lipid micelles and highlights one of the advantages of the use of soluble NDSCs.

Discussion

Translocation of substrate by ABC exporters is believed to occur when the proteins switch from an inward- to an outward-facing conformation (58-60). However, it is unclear whether the alternated accessibility of the binding pocket is the result of large conformational changes that include association/dissociation of the NBDs, where the NBDs can be tens of Å apart (monomer/dimer models) (30-33,61,62), or smaller conformational changes at the NBD-NBD interface, with the NBDs remaining associated during the transport cycle (constant-contact models) or in close proximity (34-38,61,63). The main evidence supporting a large distance between the NBDs of Pgp in the apo state comes from X-ray crystal structures in the inward-facing conformation (6-10,51), which may not be physiologically relevant (18,25,37,61,64-66). Therefore, we decided to investigate the degree of separation of the NBDs during the ATP-hydrolysis cycle of Pgp using LRET under near-physiological conditions: using a fully-active Pgp mutant reconstituted in a lipid bilayer and studied at 37°C in the absence and presence of a transport substrate, including studies during hydrolysis.

Under all conditions studied, in the absence or presence of transport substrate, in detergent or reconstituted in NDSCs, at 20°C or 37°C, Pgp adopted two dominant conformations. One of the Pgp conformations displays a donor/acceptor distance of ~33 Å (d1), and the other conformation displays a donor/acceptor distance that was longer than d1 (d2) by an average of ~10 to ~25 Å, depending on the experimental conditions. It seems reasonable to assume that d1 corresponds to the closed NBD dimer because it is close to the distance expected between the probes in the nucleotide-bound Pgp model, where the distance between the α carbons of N607 and T1252 is ~36 Å (Fig. 1) (47). This close correspondence between Cys α carbons and calculated LRET distance (within 3 Å) is a common finding for LRET-based measurements, and is likely the result of the position of the probes on the outside of the NBD structure, away from other areas of the Pgp, and the unpolarized long lifetime of the LRET sensitized emission that allows the probes to sample all orientations, centered close to the α carbon (40,41,43,44).

The longer d2 (Δ_{d2-d1} ~25 Å) was calculated for Pgp in detergent, at 20°C, in the absence of Ver. The NBD-NBD separation in detergent and in the absence of transport substrate is consistent with that in crystal structures (6,7). The shorter d2 (Δ_{d2-d1} ~10 Å) was calculated for Pgp in NDSCs in the presence of Ver and at 37°C, and it is compatible with NBDs loosely-associated or barely dissociated. These data are in agreement with an electron microscopy study of Pgp in two-dimensional lipid crystals showing NBDs close to each other even in the absence of nucleotide (25). A close proximity between the “dissociated” NBDs was also found for MsbA in NDSCs *vs.* detergent (18). Together, the data suggest that the large separation of the NBDs in the crystal structures is the result of studying the proteins under non-physiological conditions, and that in a lipid bilayer Pgp adopts a partially-open conformation with NBDs that are never far apart.

Although the inward-facing open conformation with widely separated NBDs has been observed in structures such as those of MsbA and Pgp (6,7,67), its physiologic relevance is unclear (18,66). A recent study of Pgp using DEER spectroscopy agrees with the view of a large separation between the NBDs in the apo state (22). In this study, the protein was studied “locked” in different states during the hydrolysis cycle. Although, we do not know the origin of the differences with our work, there are several potential reasons besides the methodologies employed. One is the study of Pgp in NDSCs *vs.* detergent/lipid micelles. We and others have shown that Pgp in detergent/lipid micelles behaves closer to Pgp in a lipid bilayer than the protein in detergent, but still shows significantly lower affinity for substrates (68) (Supplementary Fig. 2). Another difference is the CL Pgp version used. The CL Pgp used in the DEER spectroscopy work is an older version that we no longer use because of its reduced stability and profound alterations in drug transport ability (46,69). In this work, we used our newer CL Pgp, generated by directed evolution, which has wild-type-like properties (46). Also, the drug-stimulated activity reported in the DEER study was low (22), varying between ~3 and 20% of the values we report here. One of the most striking differences, however, is the absence of significant conformational changes in all the

conditions studied, except for the Vi state (22). This is in sharp contrast with our studies, where we found differences between all states with Pgp in NDSC at 37°C; the results in the DEER study are reminiscent of our finding of Pgp in detergent or in NDSCs at low temperature in the absence of substrate (see Fig. 6).

Recently, we found that the degree of the NBD-NBD separation in the bacterial Pgp homolog MsbA was significantly smaller than that predicted from the X-ray crystal structures (18,40). More importantly, we found significant differences between MsbA reconstituted in a lipid bilayer and MsbA in detergent (18,40). The NBDs of MsbA in NDSCs barely dissociate if they do at all, and ~50% of the molecules displayed closed NBD dimers in the apo state (18). We suggested that the structural differences between the crystal structures of MsbA and MsbA in a lipid bilayer were the result of the presence of the membrane (18). Similarities between the related exporters Pgp and MsbA are expected, however, mechanistic differences are also possible. For example, MsbA has a high basal ATPase activity that is only marginally stimulated by the transport substrate lipid A (70-72), a behavior very different from that of Pgp (73), making extrapolation of MsbA data to Pgp uncertain.

The fact that Pgp and MsbA reconstituted in a lipid bilayer share a similar separation of the NBDs in the open conformation (d2) is not surprising considering that they are homologous ABC exporters that can transport similar substrates (74). However, there were significant differences between the two proteins in the relative proportion of molecules that adopt the closed NBD dimer conformation *vs.* the open NBDs conformation. In the ATP-bound state ~70% of MsbA molecules display closed NBD dimers (45), whereas under identical experimental conditions only ~40% of Pgp molecules adopted that conformation. The difference was even more pronounced in the apo state, where the % of MsbA and Pgp molecules displaying closed NBD dimers were ~50 and ~10%, respectively. These observations are consistent with the lower probability of finding Pgp in the outward-facing conformation in an electron microscope study of MsbA and Pgp stabilized with amphiphiles (27). Mass spectrometry data also suggest that Pgp exists

predominately in the inward-facing conformation (75). It has been proposed that the preference of Pgp for the inward-facing conformation when compared to Sav1866 (34) is the result of a relative larger hydrophobicity of the drug-binding pocket and an increased charge density of the NBDs interface (47).

One unique aspect of our studies is that we could observe conformational changes of Pgp reconstituted in a bilayer while it is hydrolyzing ATP at 37°C, and in the absence or presence of the transport substrate Ver. During ATP hydrolysis in the presence of Ver, Pgp adopted a more compact NBD conformation than in the absence of Ver, and also displayed a higher % of molecules with closed NBD dimers (d1 ~40%), the closest to that of the Vi state. Since the Vi state could correspond to a semi-open, asymmetric NBDs dimer, with MgADP•Vi trapped in one closed site and the other site open (58), given the similarity between the Ver/MgATP and Vi states, it seems possible that a similar conformation is dominant in the Ver/MgATP state during Ver-stimulated hydrolysis. An alternative explanation is that the results arise from a mixture consisting of Pgp molecules with closed NBD dimers and Pgp molecules with partially-dissociated NBDs. However, this last possibility will be harder to reconcile with the ability of Pgp to trap nucleotides with a stoichiometry of one *per* Pgp in the Vi state with nearly complete inhibition of ATPase activity (69). Unfortunately, there is not available structural information for Pgp or other ABC exporters in an asymmetric dimer conformation with nucleotide trapped in only one site. Such structural information would allow us to determine if the short d2 measured in the Ver/MgATP and Vi states could correspond to an asymmetric dimer.

In general, our results agree with Cys cross-linking studies that showed that the C-terminal ends of the two Pgp NBDs do not need to separate significantly during the drug-stimulated catalytic cycle (52) and that Ver activates ATP hydrolysis by bringing the NBDs together (53). Our data also agree with a FRET study of Pgp in liposomes that included single-molecule recordings (65), where it was proposed that the Ver-stimulated catalytic cycle proceeds *via* a series of relatively small steps. Our results also suggest that the

mechanisms of basal and drug-stimulated ATPase activity are different, consistent with biochemical studies (58), and that drugs stimulate Pgp ATPase activity by a combination of reducing the NBD-NBD distance and increasing the % of the molecules with closed NBD dimers. It seems likely that during Ver-stimulated ATP hydrolysis the NBDs do not dissociate completely (or barely dissociate), as observed during ATP hydrolysis in the absence of drug.

The existence of effects of Ver binding on the NBDs is in agreement with prior reports (53,76-78). The conformational effects resulting from Ver binding to Pgp were observed at 20°C and 37°C, but required reconstitution in a lipid bilayer. Transition from the apo state to the Ver-bound state did not produce noticeable effects when Pgp was studied in detergent micelles. This observation agrees with data showing that Pgp responds to vinblastine and Ver when it is reconstituted in liposomes, but not when it is in detergent (57). Possible interpretations include masking of the substrate binding pocket by detergent and structural alterations that prevent the conformational changes needed for substrate-induced activation. Recent results showed a major effect of the Pgp substrate-binding pocket environment on the response to ligand binding (68). In that study, Pgp in n-dodecyl- β -D-maltopyranoside (DDM) displayed reduced affinity for Ver compared to the protein in liposomes, and even turned high-affinity inhibitors such as tariquidar into low-affinity activators (68). In our hands, the EC₅₀ for stimulation of Pgp ATPase activity by Ver in the NDSCs was low ($1.5 \pm 0.1 \mu\text{M}$; $n = 3$; see Supplementary Fig. 2), and similar to that reported in membranes and proteoliposomes (68). It has also been suggested that detergent partially unfolds Pgp, reducing the coupling between the drug-binding sites and the catalytic domains (79). Addition of phospholipids increases the thermal stability of Pgp (73) and appears to assist Pgp refolding into a more native conformation in which coupling between the drug binding site and the NBD is restored (77). A recent crosslinking study in Pgp has suggested that the presence of lipids is important for the communication between the NBDs and transmembrane domains required for activation of the ATPase activity (80). Our results suggest that

addition of lipids to the detergent-solubilized Pgp promoted a conformation with closer NBDs. The lack of conformational effects in response to drug binding without lipids could explain the absence of structural changes in the crystal structures of drug-free vs. drug-bound Pgp (6).

In summary, our results reconcile different models that have been proposed to explain the mechanism of Pgp and present new structural information that contributes to our understanding of the molecular mechanism of stimulation of the Pgp ATPase activity by transport substrates. We found that in the absence of transport substrate Pgp operates in a monomer/dimer mode. However, the separation between the NBDs is smaller than that found in crystal structures (6-10). Comparison of data from Pgp in NDSCs vs. detergent suggest that the inward-facing conformation in the crystal structures does not correspond to a physiologic conformation and is, at least in part, the result of the absence of the membrane. However, at this point we cannot rule out larger NBD-NBD separations under conditions such as binding of large substrates (*e.g.*, β amyloid). In the presence of substrate, Pgp seems to switch to a mode where the NBDs remain either associated (asymmetric dimer) or in close proximity during the hydrolysis cycle, which could account for the drug-stimulated ATPase activity. It is tempting to speculate that the monomer/dimer mechanism that would take place when Pgp displays basal ATPase activity switches in the presence of Ver to a constant-contact mode of operation or a mode where the NBDs separate less. In this mode, the NBDs would never dissociate completely, or would barely dissociate, which could account for the drug-stimulated ATPase activity.

Experimental Procedures

Construction of Pgp mutants-For expression in *S. cerevisiae*, codon-optimized mouse Pgp (*abcb1a*, *mdr1a*, GenBank JF834158) in the pVT expression vector (pVT-*opti-mdr3*) was used as template to generate a fully-functional CL Pgp (46,73). A tobacco etch virus (TEV) protease site (ENLYFQ), a FLAG epitope (DYKDDDDK), and a His₆ tag were added to the Pgp C-terminus immediately downstream of the *mdr1a* ORF. The FLAG, TEV and His tag sequences, underlined in the 5' to 3' sense strand, in order, were: 5'-CTCGAGGAAACTTGTACTTCCAGGGTGGT

GGAGGTTCTGGTGGTTCTGACTACAAGGAT
 GACGATGACAAGGGCGCCTCTGGTGGTTC
 TCACCACCATCACCACCATTGA-3'. A wild-type Pgp (WT Pgp) plasmid containing the same TEV, FLAG and His-tag sequences was also constructed. The new CL Pgp construct was used as template to generate two mutants by directed recombination-assisted mutagenesis (81): N607C/T1252C Pgp (NT Pgp) and NT/E1197A. The former is a catalytically-active double-Cys mutant, and the latter is a NBD2 catalytic carboxylate mutant (E1197A) based on NT Pgp. Using the last mutant as template, PCR-based mutagenesis was used to mutate the NBD1 catalytic carboxylate (E552) to generate the catalytically-inactive NT/E552A/E1197A mutant (NT/AA Pgp). Plasmids sequences were confirmed by DNA sequencing. For expression in *Pichia pastoris*, DNA sequences coding for CL Pgp, NT Pgp or NT/AA Pgp were subcloned into the pLIC-CL-*opti-mdr3*-His₆ vector as described (73), and the FLAG epitope was replaced by a double Strep II tag (WSHPQFEK) that is more cost-effective for large-scale purifications.

Drug resistance assay-Plasmids were transformed into *S. cerevisiae* strain JP201 and drug resistance assays were performed as previously described (73,82).

Pgp expression and purification-For purification from *S. cerevisiae*, plasmids were transformed into the BY4743 strain provided by Dr. B.L. Schneider (83). Fourteen-l cultures were grown in a New Brunswick BioFlow IV fermentor to a maximal OD₆₀₀ of 4.0, which produce 100-120 g of cells. Microsomal membrane preparation, Pgp solubilization in 0.6% DDM and purification based on the affinity of the Pgp His₆ tag for Ni-NTA were performed as described (46,73). Pgp was eluted from the Ni-NTA resin with buffer A (250 mM NaCl, 10% glycerol, 0.1% DDM, 1 mM β -mercaptoethanol, 0.1 mM tris(2-carboxyethyl) phosphine (TCEP) and 50 mM Tris/HCl, pH 7.4) containing 200 mM imidazole. A second purification step was performed by binding the imidazole eluate containing Pgp to an anti-FLAG M2 affinity gel (A2220, Sigma-Aldrich, St. Louis, MO), with elution by competition in buffer A containing 100 μ g/ml FLAG peptide; the reducing agent TCEP was omitted from all anti-FLAG gel buffers. Pgp concentrated to ~1.5 mg/ml using

100-kDa cut-off centrifugal filter units (Amicon, EMD Millipore, Billerica, MA) was stored in aliquots at -80°C until used. Protein concentration was calculated from the absorbance at 280 nm using a Pgp molar extinction coefficient of 109,750 M⁻¹cm⁻¹.

For larger-scale expression we used the *P. pastoris* strain KM71H. Cells transformed with the corresponding expression plasmids were grown in 6- to 8-l fermentor cultures, and were induced with methanol (46,73,84). The first purification step was based on Pgp affinity for the Ni-NTA resin (see above). Pgp was subjected to an additional purification step consisting of binding to a streptactin superflow resin (Qiagen, Valencia, CA) in buffer A with 1 mM DTT, with elution by competition with 2.5 mM desthiobiotin. We did not detect biochemical differences between Pgp expressed and purified from *S. cerevisiae* and *P. pastoris* expression/purification tag systems.

Labeling of Pgp and reconstitution into nanodiscs-Purified CL Pgp, NT Pgp and NT/AA Pgp mutant proteins were first reduced with 1 mM DTT for 15 min on ice, followed by removal of most DTT using 1-ml Sephadex G50 spin columns (85) or Zeba columns (ThermoFisher Sci., Bellafonte, PA) pre-equilibrated in buffer A without TCEP. Pgp was then labeled with a two-fold molar excess (2:1 dye:Cys) of both, donor (Tb³⁺-chelate DTPA-cs124-EMPH; thiol-reactive Lanthascreen, Life Technologies, Carlsbad, CA) (86) and acceptor (Bodipy FL *N*-(2-aminoethyl)maleimide; Bodipy FL maleimide, Life Technologies) for 1 h at room temperature. For some experiments, NT Pgp was labeled only with donor or acceptor. Bodipy FL/Pgp stoichiometry, estimated from the absorbances of Pgp (280 nm) and Bodipy FL (504 nm; using a Bodipy FL molar extinction coefficient of 84,000 M⁻¹cm⁻¹) was ~0.6 mol/mol when NT Pgp was labeled with donor and acceptor and or ~1.2 when it was labeled only with Bodipy FL. Compared to NT Pgp and NT/AA Pgp, CL Pgp showed essentially no labeling under the conditions described above, consisting with our previous studies (46). For LRET experiments of Pgp in detergent, the unreacted free labels were removed by size exclusion chromatography on a Superdex 200 column (3.2/30 mm, GE Healthcare, Piscataway, NJ) equilibrated with buffer A.

Alternatively, labeled Pgp was reconstituted in NDSCs following previously described procedures (18,39). Pgp in detergent micelles has very low ATPase activity at 20-25°C, and its activity at 37°C decreases rapidly ($t_{1/2} \sim 5$ min). Supplementation of the detergent-solubilized protein with lipids increases the thermo-stability of Pgp (Supplementary Fig. 3) (73), but light scattering hinders the detection of fluorescence changes. Therefore, we decided to study Pgp in lipid NDSCs using LRET, an approach that we used successfully to study MsbA (18,40). For reconstitution in NDSCs, labeled Pgp, *E. coli* polar lipids (Avanti Polar Lipids, Alabaster, AL) and the membrane scaffold protein MSP1E3D1 were mixed (at a molar ratio of 1:6 Pgp:MSP; and 1:110 MSP:lipids). The mixture was incubated for 1 h at 4°C, and then the detergent was removed by overnight incubation with Bio-Beads SM-2 (Bio-Rad). The NDSC sample was run on a Superdex 200 column (10/300 mm) equilibrated with detergent-free NDSC buffer (150 mM NaCl, 0.1 mM TCEP, 50 mM Tris HCl pH 7.4) to remove free unreacted labels, and to isolate a fraction enriched in Pgp-loaded NDSCs (Fig. 2B, black). For some experiments, Pgp-NDs were further separated from empty NDSCs by anti-FLAG affinity chromatography as described above, except that detergent-free NDSC buffer was used for binding, washing and elution (Fig. 2B, red). Pgp concentration in the NDSC preparation was determined in SDS-PAGE gels stained with Coomassie blue, using known amounts of detergent-solubilized Pgp as standard.

As expected from the absence of Cys in MSP1E3D1, the results using NT Pgp labeled with the LRET probes after reconstitution in NDSCs were identical to those obtained using NT Pgp labeled in detergent and then reconstituted in NDSCs.

LRET studies-For LRET studies, ~ 1 μ M of CL Pgp, NT Pgp or NT/AA Pgp subjected to the labeling protocol, in either detergent or NDSCs, were analyzed in 3 mm-pathlength quartz cuvettes, essentially as described (40,41,45). The samples were first analyzed in nucleotide- and drug-free state (**apo state**) using NDSC buffer with 1 mM EDTA to chelate trace divalent cations and prevent ATP hydrolysis. Then, the samples were analyzed after successive additions of NaATP (5

mM NaATP; **ATP-bound state**), MgSO₄ (10 mM MgSO₄; **MgATP**; during continuous ATP hydrolysis) and sodium orthovanadate (0.25 mM Vi; **Vi state**; post-hydrolysis intermediate state). We used 30 μ M Ver to determine the effect of binding of transport substrate. Emission spectra (QM3SS spectrometer; Photon Technology International, London, Canada), LRET decays and intensity time courses (EasyLife L phosphorescence lifetime photometer, Optical Building Blocks, NJ) were recorded as described (18,41,50,87). Emission was acquired with a 200- μ s delay from the beginning of the ~ 1 - μ s excitation pulse from a xenon flash lamp (gated mode). This 200- μ s delay allows for the selective recording of long-lifetime processes (donor emission or sensitized emission from the acceptor) after the short-lifetime processes (e.g., acceptor emission resulting from direct excitation, and scattering of the excitation pulse) have largely disappeared. Excitation was set to 335 nm and emission was collected through bandpass filters (Tb³⁺: 490/10 nm; Bodipy FL: 520/10 nm, Omega Optical, Brattleboro, VT) or an emission monochromator. As expected, control experiments mixing equal proportions of NT Pgp labeled with Tb³⁺-only and Bodipy FL-only showed essentially no intermolecular LRET. LRET experiments were performed at 37°C unless stated otherwise.

LRET decay analysis-Donor/acceptor distances were calculated according to: $E = 1 - \tau_{DA}/\tau_D$, and $R = R_0 (E^{-1}-1)^{1/6}$, where E is the efficiency of energy transfer, τ_D is the lifetime of the donor in the absence of acceptor, τ_{DA} is the sensitized emission lifetime (lifetime of the acceptor that arises from LRET), R is the donor-acceptor distance, and R_0 is the Förster distance (the distance at which E = 0.5). The R_0 determined for the Tb³⁺/Bodipy FL pair was 41 Å, making this LRET pair very sensitive to distances changes in the ~ 30 -55 Å range; Supplementary Fig. 4).

The donor-only decay from NT Pgp produced in *S. cerevisiae*, without the strep tag, or in *P. pastoris*, studied after removal of the tag with TEV protease, were undistinguishable. The Tb³⁺ emission decays recorded at 490 ± 10 nm and at 37°C were well fitted by a 2-exponential function with lifetimes of 722 ± 5 μ s (τ_{D1} ; 5% of the signal) and $1,850 \pm 10$ μ s (τ_{D2} ; 95% of the signal) (n = 6). This longest Tb-only lifetime (τ_{D2}) was used as the

donor-only τ_D . The donor-only τ_{D2} from NT Pgp with the strep-tag was shorter ($1,517 \pm 11 \mu\text{s}$; $n = 3$), but returned to the normal value after removal of the tag with TEV protease. Therefore, for the LRET experiments the strep tag from NT Pgp expressed in *P. pastoris* was removed with TEV protease as described (88). At 20°C τ_{D2} lengthened to $2,204 \pm 37 \mu\text{s}$ ($n = 3$).

The sensitized emission decays from Bodipy FL, recorded at $520 \pm 10 \text{ nm}$, were well fitted by a 3-exponential decay function. This function was chosen by the improving of the fitting from the 2- to the 3-exponential function, without significant additional improvement in the goodness of fit by fitting a 4-exponential function to the data. The goodness of fit with the increase from 2 to 4 exponential components was assessed by the decreases in χ^2 and the value of weighted residuals, a random distribution of weighted residuals, and a rapid decay of the autocorrelation of weighted residuals. Once χ^2 did not change appreciably by increasing the number of parameters (fitting from 3 to 4 exponentials), we performed a one-sided *F*-test of sample variance (s^2) with null (H_0 : $s^2_{3\text{-exp}} = s^2_{4\text{-exp}}$) and alternative (H_a : $s^2_{3\text{-exp}} > s^2_{4\text{-exp}}$) hypotheses. With $s^2_{3\text{-exp}}/s^2_{4\text{-exp}}$ typically < 1.005 , H_a was rejected ($P < 0.001$). The fastest component of the 3-exponential fits (τ_{DA} 100-200 μs) accounted for $\leq 5\%$ of the signal and was disregarded for the calculations because it did not change appreciably under different experimental conditions, and is largely the consequence of the instrument response time (40,41,45). The presence of only 2 relevant exponential decay components was also apparent from the analysis of lifetimes distribution using an exponential series method designed to recover

lifetime distributions without *a priori* assumptions about their shapes (see below) (54).

The percentage of donor-acceptor pairs with a discrete average distance (percentage Pgp molecules in each conformation) was estimated from the relative intensity of each lifetime component and the rate of energy transfer ($k = 1/\tau_{DA} - 1/\tau_D$) as described (40,45,89). Analysis of the distribution of lifetimes and distances was performed by an exponential series method (Felix 32 analysis software, PTI) designed to recover lifetime distributions without *a priori* assumptions about their shapes (54). We analyzed the decays using a series of 200 exponentials with fixed, logarithmically-spaced lifetimes and variable pre-exponentials. The use of logarithmically-spaced lifetimes assigns more points to shorter lifetimes, which can be visually misleading regarding the relative proportion of molecules in different conformations. To minimize this effect, areas under the peaks were normalized to the cumulative percentage of molecules, also calculated by the exponential series method. Average data without normalization, in the presence of Ver, and the corresponding percentage cumulative distances data are presented in Supplementary Fig. 8.

ATPase activity assays-Purified Pgp (0.5-1.0 μg) in detergent was activated by incubation with 10 mM DTT and 1% (w/v) *E. coli* polar lipids for 15 min at room temperature. For Pgp in NDSCs, the protein (0.5-1.0 μg) was directly diluted into the assay cocktail without DTT or lipid. The rate of ATP hydrolysis was measured at 37°C by an ATPase linked enzyme assay, as described (73), in the absence and presence of 30 μM Ver.

Acknowledgements: We thank the Center for Membrane Protein Research members (<http://www.ttuhsu.edu/cmpr/>) and Dr. Qinghai Zhang (The Scripps Research Institute, La Jolla, CA) for critical discussions.

Conflict of interest: The authors declare that they have no conflicts of interest with the contents of this article.

Author contributions: MEZ, LM, ILU and GAA conceived and designed the study, and analyzed and interpreted the data. ILU, DJS, LM and AS developed the expression, purification and labeling protocols of highly active CL and NT Pgp, and analyzed temperature-sensitive ATPase activity of detergent-soluble and reconstituted Pgp. GAF made the NT/AA mutant. GAA, MEZ and LM performed most LRET experiments and analyzed LRET data. MEZ, ILU and GAA wrote the manuscript.

References

1. Sharom, F. J. (2011) The P-glycoprotein multidrug transporter. *Essays Biochem* **50**, 161-178
2. Gottesman, M. M., and Ling, V. (2006) The molecular basis of multidrug resistance in cancer: the early years of P-glycoprotein research. *FEBS Lett* **580**, 998-1009
3. Eckford, P. D., and Sharom, F. J. (2009) ABC efflux pump-based resistance to chemotherapy drugs. *Chem Rev* **109**, 2989-3011
4. International Transporter, C., Giacomini, K. M., Huang, S. M., Tweedie, D. J., Benet, L. Z., Brouwer, K. L., Chu, X., Dahlin, A., Evers, R., Fischer, V., Hillgren, K. M., Hoffmaster, K. A., Ishikawa, T., Keppler, D., Kim, R. B., Lee, C. A., Niemi, M., Polli, J. W., Sugiyama, Y., Swaan, P. W., Ware, J. A., Wright, S. H., Yee, S. W., Zamek-Gliszczynski, M. J., and Zhang, L. (2010) Membrane transporters in drug development. *Nat Rev Drug Discov* **9**, 215-236
5. U.S. Food and Drug Administration, C. f. D. E. a. R. (2012) Guidance for industry: drug interaction studies - study design, data analysis, implications for dosing, and labeling recommendations.
<http://www.fda.gov/downloads/Drugs/GuidanceComplianceRegulatoryInformation/Guidances/ucm292362.pdf>
6. Aller, S. G., Yu, J., Ward, A., Weng, Y., Chittaboina, S., Zhuo, R., Harrell, P. M., Trinh, Y. T., Zhang, Q., Urbatsch, I. L., and Chang, G. (2009) Structure of P-glycoprotein reveals a molecular basis for poly-specific drug binding. *Science* **323**, 1718-1722
7. Li, J., Jaimes, K. F., and Aller, S. G. (2014) Refined structures of mouse P-glycoprotein. *Protein Sci* **23**, 34-46
8. Ward, A. B., Szewczyk, P., Grimard, V., Lee, C. W., Martinez, L., Doshi, R., Caya, A., Villaluz, M., Pardon, E., Cregger, C., Swartz, D. J., Falson, P. G., Urbatsch, I. L., Govaerts, C., Steyaert, J., and Chang, G. (2013) Structures of P-glycoprotein reveal its conformational flexibility and an epitope on the nucleotide-binding domain. *Proc Natl Acad Sci USA* **110**, 13386-13391
9. Jin, M. S., Oldham, M. L., Zhang, Q., and Chen, J. (2012) Crystal structure of the multidrug transporter P-glycoprotein from *Caenorhabditis elegans*. *Nature* **490**, 566-569
10. Szewczyk, P., Tao, H., McGrath, A. P., Villaluz, M., Rees, S. D., Lee, S. C., Doshi, R., Urbatsch, I. L., Zhang, Q., and Chang, G. (2015) Snapshots of ligand entry, malleable binding and induced helical movement in P-glycoprotein. *Acta Crystallogr D Biol Crystallogr* **71**, 732-741
11. Hollenstein, K., Dawson, R. J., and Locher, K. P. (2007) Structure and mechanism of ABC transporter proteins. *Curr Opin Struct Biol* **17**, 412-418
12. Loo, T. W., Bartlett, M. C., and Clarke, D. M. (2010) Human P-glycoprotein is active when the two halves are clamped together in the closed conformation. *Biochem Biophys Res Commun* **395**, 436-440
13. Loo, T. W., and Clarke, D. M. (2014) Identification of the distance between the homologous halves of P-glycoprotein that triggers the high/low ATPase activity switch. *J Biol Chem* **289**, 8484-8492
14. Qu, Q., and Sharom, F. J. (2001) FRET analysis indicates that the two ATPase active sites of the P-glycoprotein multidrug transporter are closely associated. *Biochemistry* **40**, 1413-1422

15. Borbat, P. P., Surendhran, K., Bortolus, M., Zou, P., Freed, J. H., and McHaourab, H. S. (2007) Conformational motion of the ABC transporter MsbA induced by ATP hydrolysis. *PLoS Biol* **5**, e271
16. Cooper, R. S., and Altenberg, G. A. (2013) Association/dissociation of the nucleotide-binding domains of the ATP-binding cassette protein MsbA measured during continuous hydrolysis. *J Biol Chem* **288**, 20785-20796
17. Verhalen, B., Ernst, S., Borsch, M., and Wilkens, S. (2012) Dynamic ligand-induced conformational rearrangements in P-glycoprotein as probed by fluorescence resonance energy transfer spectroscopy. *J Biol Chem* **287**, 1112-1127
18. Zoghbi, M. E., Cooper, R. S., and Altenberg, G. A. (2016) The lipid bilayer modulates the structure and function of an ATP-binding cassette exporter. *J Biol Chem* **291**, 4453-4461
19. Zou, P., Bortolus, M., and McHaourab, H. S. (2009) Conformational cycle of the ABC transporter MsbA in liposomes: detailed analysis using double electron-electron resonance spectroscopy. *J Mol Biol* **393**, 586-597
20. Wen, P. C., Verhalen, B., Wilkens, S., McHaourab, H. S., and Tajkhorshid, E. (2013) On the origin of large flexibility of P-glycoprotein in the inward-facing state. *J Biol Chem* **288**, 19211-19220
21. van Wonderen, J. H., McMahon, R. M., O'Mara, M. L., McDevitt, C. A., Thomson, A. J., Kerr, I. D., MacMillan, F., and Callaghan, R. (2014) The central cavity of ABCB1 undergoes alternating access during ATP hydrolysis. *FEBS J* **281**, 2190-2201
22. Verhalen, B., Dastvan, R., Thangapandian, S., Peskova, Y., Koteiche, H. A., Nakamoto, R. K., Tajkhorshid, E., and McHaourab, H. S. (2017) Energy transduction and alternating access of the mammalian ABC transporter P-glycoprotein. *Nature* **543**, 738-741
23. Marcoux, J., Wang, S. C., Politis, A., Reading, E., Ma, J., Biggin, P. C., Zhou, M., Tao, H., Zhang, Q., Chang, G., Morgner, N., and Robinson, C. V. (2013) Mass spectrometry reveals synergistic effects of nucleotides, lipids, and drugs binding to a multidrug resistance efflux pump. *Proc Natl Acad Sci USA* **110**, 9704-9709
24. Lee, J. Y., Urbatsch, I. L., Senior, A. E., and Wilkens, S. (2002) Projection structure of P-glycoprotein by electron microscopy. Evidence for a closed conformation of the nucleotide binding domains. *J Biol Chem* **277**, 40125-40131
25. Lee, J. Y., Urbatsch, I. L., Senior, A. E., and Wilkens, S. (2008) Nucleotide-induced structural changes in P-glycoprotein observed by electron microscopy. *J Biol Chem* **283**, 5769-5779
26. Fribourg, P. F., Chami, M., Sorzano, C. O., Gubellini, F., Marabini, R., Marco, S., Jault, J. M., and Levy, D. (2014) 3D cryo-electron reconstruction of BmrA, a bacterial multidrug ABC transporter in an inward-facing conformation and in a lipidic environment. *J Mol Biol* **426**, 2059-2069
27. Moeller, A., Lee, S. C., Tao, H., Speir, J. A., Chang, G., Urbatsch, I. L., Potter, C. S., Carragher, B., and Zhang, Q. (2015) Distinct conformational spectrum of homologous multidrug ABC transporters. *Structure* **23**, 450-460
28. Smith, P. C., Karpowich, N., Millen, L., Moody, J. E., Rosen, J., Thomas, P. J., and Hunt, J. F. (2002) ATP binding to the motor domain from an ABC transporter drives formation of a nucleotide sandwich dimer. *Mol Cell* **10**, 139-149
29. Hopfner, K. P., Karcher, A., Shin, D. S., Craig, L., Arthur, L. M., Carney, J. P., and Tainer, J. A. (2000) Structural biology of Rad50 ATPase: ATP-driven conformational

- control in DNA double-strand break repair and the ABC-ATPase superfamily. *Cell* **101**, 789-800
30. Higgins, C. F. (2007) Multiple molecular mechanisms for multidrug resistance transporters. *Nature* **446**, 749-757
 31. Janas, E., Hofacker, M., Chen, M., Gompf, S., van der Does, C., and Tampe, R. (2003) The ATP hydrolysis cycle of the nucleotide-binding domain of the mitochondrial ATP-binding cassette transporter Mdl1p. *J Biol Chem* **278**, 26862-26869
 32. Vergani, P., Lockless, S. W., Nairn, A. C., and Gadsby, D. C. (2005) CFTR channel opening by ATP-driven tight dimerization of its nucleotide-binding domains. *Nature* **433**, 876-880
 33. Oswald, C., Holland, I. B., and Schmitt, L. (2006) The motor domains of ABC-transporters. What can structures tell us? *Naunyn Schmiedebergs Arch Pharmacol* **372**, 385-399
 34. Dawson, R. J., and Locher, K. P. (2006) Structure of a bacterial multidrug ABC transporter. *Nature* **443**, 180-185
 35. Jones, P. M., and George, A. M. (2007) Nucleotide-dependent allostery within the ABC transporter ATP-binding cassette: a computational study of the MJ0796 dimer. *J Biol Chem* **282**, 22793-22803
 36. Jones, P. M., and George, A. M. (2011) Molecular-dynamics simulations of the ATP/apo state of a multidrug ATP-binding cassette transporter provide a structural and mechanistic basis for the asymmetric occluded state. *Biophys J* **100**, 3025-3034
 37. Jones, P. M., and George, A. M. (2009) Opening of the ADP-bound active site in the ABC transporter ATPase dimer: evidence for a constant contact, alternating sites model for the catalytic cycle. *Proteins* **75**, 387-396
 38. Sauna, Z. E., Kim, I. W., Nandigama, K., Kopp, S., Chiba, P., and Ambudkar, S. V. (2007) Catalytic cycle of ATP hydrolysis by P-glycoprotein: evidence for formation of the E.S reaction intermediate with ATP-gamma-S, a nonhydrolyzable analogue of ATP. *Biochemistry* **46**, 13787-13799
 39. Ritchie, T. K., Grinkova, Y. V., Bayburt, T. H., Denisov, I. G., Zolnerciks, J. K., Atkins, W. M., and Sligar, S. G. (2009) Chapter 11 - Reconstitution of membrane proteins in phospholipid bilayer nanodiscs. *Methods Enzymol* **464**, 211-231
 40. Cooper, R. S., and Altenberg, G. A. (2013) Association/dissociation of the nucleotide-binding domains of the ATP-binding cassette protein MsbA measured during continuous hydrolysis. *J Biol Chem* **288**, 20785-20796
 41. Zoghbi, M. E., Krishnan, S., and Altenberg, G. A. (2012) Dissociation of ATP-binding cassette nucleotide-binding domain dimers into monomers during the hydrolysis cycle. *J Biol Chem* **287**, 14994-15000
 42. Zoghbi, M. E., Fuson, K. L., Sutton, R. B., and Altenberg, G. A. (2012) Kinetics of the association/dissociation cycle of an ATP-binding cassette nucleotide-binding domain. *J Biol Chem* **287**, 4157-4164
 43. Posson, D. J., Ge, P., Miller, C., Bezanilla, F., and Selvin, P. R. (2005) Small vertical movement of a K⁺ channel voltage sensor measured with luminescence energy transfer. *Nature* **436**, 848-851
 44. Selvin, P. R. (2002) Principles and biophysical applications of lanthanide-based probes. *Annu Rev Biophys Biomol Struct* **31**, 275-302

45. Zoghbi, M. E., Cooper, R. S., and Altenberg, G. A. (2016) The lipid bilayer modulates the structure and function of an ATP-binding cassette exporter. *J Biol Chem*
46. Swartz, D. J., Mok, L., Botta, S. K., Singh, A., Altenberg, G. A., and Urbatsch, I. L. (2014) Directed evolution of P-glycoprotein cysteines reveals site-specific, non-conservative substitutions that preserve multidrug resistance. *Biosci Rep* **34**
47. Pan, L., and Aller, S. G. (2015) Equilibrated atomic models of outward-facing P-glycoprotein and effect of ATP binding on structural dynamics. *Sci Rep* **5**, 7880
48. Tomblin, G., Bartholomew, L. A., Urbatsch, I. L., and Senior, A. E. (2004) Combined mutation of catalytic glutamate residues in the two nucleotide binding domains of P-glycoprotein generates a conformation that binds ATP and ADP tightly. *J Biol Chem* **279**, 31212-31220
49. Urbatsch, I. L., Tyndall, G. A., Tomblin, G., and Senior, A. E. (2003) P-glycoprotein catalytic mechanism: studies of the ADP-vanadate inhibited state. *J Biol Chem* **278**, 23171-23179
50. Zoghbi, M. E., and Altenberg, G. A. (2013) Hydrolysis at one of the two nucleotide-binding sites drives the dissociation of ATP-binding cassette nucleotide-binding domain dimers. *J Biol Chem* **288**, 34259-34265
51. Frank, G. A., Shukla, S., Rao, P., Borgnia, M. J., Bartesaghi, A., Merk, A., Mobin, A., Esser, L., Earl, L. A., Gottesman, M. M., Xia, D., Ambudkar, S. V., and Subramaniam, S. (2016) Cryo-EM analysis of the conformational landscape of human P-glycoprotein (ABCB1) during its catalytic cycle. *Mol Pharmacol* **90**, 35-41
52. Verhalen, B., and Wilkens, S. (2011) P-glycoprotein retains drug-stimulated ATPase activity upon covalent linkage of the two nucleotide binding domains at their C-terminal ends. *J Biol Chem* **286**, 10476-10482
53. Loo, T. W., Bartlett, M. C., and Clarke, D. M. (2003) Drug binding in human P-glycoprotein causes conformational changes in both nucleotide-binding domains. *J Biol Chem* **278**, 1575-1578
54. James, D. R., and Ware, W. R. (1986) Recovery of underlying distributions of lifetimes from fluorescence decay data. *Chem Phys Lett* **126**, 7-11
55. Siemiarz, A., Wagner, B. D., and Ware, W. R. (1990) Comparison of the maximum entropy and exponential series methods for the recovery of distributions of lifetimes from fluorescence lifetime data. *J Phys Chem* **94**, 1661-1666
56. Al-Shawi, M. K., Polar, M. K., Omote, H., and Figler, R. A. (2003) Transition state analysis of the coupling of drug transport to ATP hydrolysis by P-glycoprotein. *J Biol Chem* **278**, 52629-52640
57. Ambudkar, S. V., Lelong, I. H., Zhang, J., Cardarelli, C. O., Gottesman, M. M., and Pastan, I. (1992) Partial purification and reconstitution of the human multidrug-resistance pump: characterization of the drug-stimulatable ATP hydrolysis. *Proc Natl Acad Sci USA* **89**, 8472-8476
58. Al-Shawi, M. K. (2011) Catalytic and transport cycles of ABC exporters. *Essays Biochem* **50**, 63-83
59. Bouige, P., Laurent, D., Piloyan, L., and Dassa, E. (2002) Phylogenetic and functional classification of ATP-binding cassette (ABC) systems. *Curr Protein Pept Sci* **3**, 541-559
60. Sharom, F. J. (2008) ABC multidrug transporters: structure, function and role in chemoresistance. *Pharmacogenomics* **9**, 105-127

61. Jones, P. M., O'Mara, M. L., and George, A. M. (2009) ABC transporters: a riddle wrapped in a mystery inside an enigma. *Trends Biochem Sci* **34**, 520-531
62. Moody, J. E., Millen, L., Binns, D., Hunt, J. F., and Thomas, P. J. (2002) Cooperative, ATP-dependent association of the nucleotide binding cassettes during the catalytic cycle of ATP-binding cassette transporters. *J Biol Chem* **277**, 21111-21114
63. Jones, P. M., and George, A. M. (2013) Mechanism of the ABC transporter ATPase domains: catalytic models and the biochemical and biophysical record. *Crit Rev Biochem Mol Biol* **48**, 39-50
64. George, A. M., and Jones, P. M. (2013) An asymmetric post-hydrolysis state of the ABC transporter ATPase dimer. *PLoS One* **8**, e59854
65. Verhalen, B., Ernst, S., Borsch, M., and Wilkens, S. (2012) Dynamic ligand-induced conformational rearrangements in P-glycoprotein as probed by fluorescence resonance energy transfer spectroscopy. *J Biol Chem* **287**, 1112-1127
66. Locher, K. P. (2016) Mechanistic diversity in ATP-binding cassette (ABC) transporters. *Nat Struct Mol Biol* **23**, 487-493
67. Ward, A., Reyes, C. L., Yu, J., Roth, C. B., and Chang, G. (2007) Flexibility in the ABC transporter MsbA: Alternating access with a twist. *Proc Natl Acad Sci USA* **104**, 19005-19010
68. Shukla, S., Abel, B., Chufan, E. E., and Ambudkar, S. V. (2017) Effects of a detergent micelle environment on P-glycoprotein (ABCB1)-ligand interactions. *J Biol Chem* **292**, 7066-7076
69. Tomblin, G., Urbatsch, I. L., Virk, N., Muharemagic, A., White, L. B., and Senior, A. E. (2006) Expression, purification, and characterization of cysteine-free mouse P-glycoprotein. *Arch Biochem Biophys* **445**, 124-128
70. Eckford, P. D., and Sharom, F. J. (2008) Functional characterization of Escherichia coli MsbA: interaction with nucleotides and substrates. *J Biol Chem* **283**, 12840-12850
71. Bretscher, L. E., Buchaklian, A. H., and Klug, C. S. (2008) Spin-labeled lipid A. *Anal Biochem* **382**, 129-131
72. Doshi, R., and van Veen, H. W. (2013) Substrate binding stabilizes a pre-translocation intermediate in the ATP-binding cassette transport protein MsbA. *J Biol Chem* **288**, 21638-21647
73. Bai, J., Swartz, D. J., Protasevich, II, Brouillette, C. G., Harrell, P. M., Hildebrandt, E., Gasser, B., Mattanovich, D., Ward, A., Chang, G., and Urbatsch, I. L. (2011) A gene optimization strategy that enhances production of fully functional P-glycoprotein in *Pichia pastoris*. *PLoS One* **6**, e22577
74. Reuter, G., Janvilisri, T., Venter, H., Shahi, S., Balakrishnan, L., and van Veen, H. W. (2003) The ATP binding cassette multidrug transporter LmrA and lipid transporter MsbA have overlapping substrate specificities. *J Biol Chem* **278**, 35193-35198
75. Marcoux, J., Wang, S. C., Politis, A., Reading, E., Ma, J., Biggin, P. C., Zhou, M., Tao, H., Zhang, Q., Chang, G., Morgner, N., and Robinson, C. V. (2013) Mass spectrometry reveals synergistic effects of nucleotides, lipids, and drugs binding to a multidrug resistance efflux pump. *Proc Natl Acad Sci USA* **110**, 9704-9709
76. Loo, T. W., Bartlett, M. C., and Clarke, D. M. (2003) Permanent activation of the human P-glycoprotein by covalent modification of a residue in the drug-binding site. *J Biol Chem* **278**, 20449-20452

77. Liu, R., and Sharom, F. J. (1996) Site-directed fluorescence labeling of P-glycoprotein on cysteine residues in the nucleotide binding domains. *Biochemistry* **35**, 11865-11873
78. Wang, G., Pincheira, R., Zhang, M., and Zhang, J. T. (1997) Conformational changes of P-glycoprotein by nucleotide binding. *Biochem J* **328** (Pt 3), 897-904
79. Sharom, F. J., Yu, X., Chu, J. W., and Doige, C. A. (1995) Characterization of the ATPase activity of P-glycoprotein from multidrug-resistant Chinese hamster ovary cells. *Biochem J* **308**, 381-390
80. Loo, T. W., and Clarke, D. M. (2016) P-glycoprotein ATPase activity requires lipids to activate a switch at the first transmission interface. *Biochem Biophys Res Commun* **472**, 379-383
81. Stindt, J., Ellinger, P., Stross, C., Keitel, V., Haussinger, D., Smits, S. H., Kubitz, R., and Schmitt, L. (2011) Heterologous overexpression and mutagenesis of the human bile salt export pump (ABCB11) using DREAM (Directed REcombination-Assisted Mutagenesis). *PLoS One* **6**, e20562
82. Beaudet, L., and Gros, P. (1995) Functional dissection of P-glycoprotein nucleotide-binding domains in chimeric and mutant proteins. Modulation of drug resistance profiles. *J Biol Chem* **270**, 17159-17170
83. Brachmann, C. B., Davies, A., Cost, G. J., Caputo, E., Li, J., Hieter, P., and Boeke, J. D. (1998) Designer deletion strains derived from *Saccharomyces cerevisiae* S288C: a useful set of strains and plasmids for PCR-mediated gene disruption and other applications. *Yeast* **14**, 115-132
84. Lerner-Marmarosh, N., Gimi, K., Urbatsch, I. L., Gros, P., and Senior, A. E. (1999) Large scale purification of detergent-soluble P-glycoprotein from *Pichia pastoris* cells and characterization of nucleotide binding properties of wild-type, Walker A, and Walker B mutant proteins. *J Biol Chem* **274**, 34711-34718
85. Urbatsch, I. L., Gimi, K., Wilke-Mounts, S., and Senior, A. E. (2000) Conserved walker A Ser residues in the catalytic sites of P-glycoprotein are critical for catalysis and involved primarily at the transition state step. *J Biol Chem* **275**, 25031-25038
86. Chen, J., and Selvin, P. R. (1999) Thiol-reactive luminescent chelates of terbium and europium. *Bioconjug Chem* **10**, 311-315
87. Zoghbi, M. E., and Altenberg, G. A. (2014) ATP binding to two sites is necessary for dimerization of nucleotide-binding domains of ABC proteins. *Biochem Biophys Res Commun* **443**, 97-102
88. Fiori, M. C., Krishnan, S., Cortes, D. M., Retamal, M. A., Reuss, L., Altenberg, G. A., and Cuello, L. G. (2015) Functional hemichannels formed by human connexin 26 expressed in bacteria. *Biosci Rep* **35**
89. Heyduk, T., and Heyduk, E. (2001) Luminescence energy transfer with lanthanide chelates: interpretation of sensitized acceptor decay amplitudes. *Anal Biochem* **289**, 60-67

Footnotes

This work was supported in part by the Cancer Prevention and Research Institute of Texas Grant RP101073, the National Institute of Health grants RGM102928 and R01GM118594, and the South Plains Foundation from Lubbock, Texas.

The abbreviations used are: ABC, ATP-binding cassette; CL, Cys-less; DDM, n-dodecyl- β -D-maltopyranoside; DEER, double electron-electron resonance; E, efficiency of energy transfer; LRET, luminescence resonance energy transfer; MSP, membrane scaffold protein; NBD, nucleotide-binding

domain; NDSC, nanodisc; NT, N607C/T1256C Pgp mutant; Pgp, P-glycoprotein; R, donor-acceptor distance; R_0 , Förster distance (the distance at which $E = 0.5$); TCEP, Tris (2-carboxyethyl) phosphine hydrochloride; τ_D , lifetime of the donor in the absence of acceptor; τ_{DA} , sensitized emission lifetime (lifetime of the acceptor that arises from LRET); Ver, verapamil; Vi, sodium orthovanadate.

TABLE 1. Distances between the Tb^{3+} and Bodipy FL probes during the catalytic cycle of NT Pgp.

NT Pgp in NDSCs in the absence of transport substrate (n = 7)						
	d1			d2		
State	τ_{DA} (μ s)	R_1 (\AA)	% molecules	τ_{DA} (μ s)	R_2 (\AA)	% molecules
Apo	378 ± 12	32.7 ± 0.2	12 ± 1	1286 ± 18	47.1 ± 0.4	88 ± 1
ATP-bound	369 ± 11	32.5 ± 0.2	40 ± 4	1212 ± 11	45.6 ± 0.2	60 ± 4
MgATP	414 ± 13	33.3 ± 0.2	29 ± 2	1282 ± 19	47.0 ± 0.4	71 ± 2
Vi	439 ± 16	33.7 ± 0.3	49 ± 4	1088 ± 34	43.6 ± 0.5	51 ± 4
NT Pgp in NDSCs in the presence of 30 μ M verapamil (Ver; n = 5)						
	d1			d2		
State	τ_{DA} (μ s)	R_1 (\AA)	% molecules	τ_{DA} (μ s)	R_2 (\AA)	% molecules
Apo	373 ± 11	32.6 ± 0.2	12 ± 1	1265 ± 37	46.7 ± 0.8	88 ± 1
Ver-bound	389 ± 16	32.9 ± 0.3	17 ± 1	1136 ± 13	44.3 ± 0.2	83 ± 1
Ver/ATP-bound	349 ± 20	32.1 ± 0.4	24 ± 3	1150 ± 11	44.5 ± 0.2	76 ± 3
Ver/MgATP	394 ± 17	33.0 ± 0.3	39 ± 4	1164 ± 33	44.8 ± 0.6	61 ± 4
Ver/Vi	430 ± 28	33.6 ± 0.5	46 ± 6	1119 ± 32	44.0 ± 2.0	54 ± 6

The measurements in the absence of Ver were obtained first for the apo state and then after sequential addition of 5 mM NaATP (ATP-bound state), 10 mM $MgSO_4$ (MgATP state) and 0.25 mM Vi (Vi state). In the presence of Ver measurements were obtained first for the apo state and then after sequential addition of Ver (Ver-bound state), 5 mM NaATP (Ver/ATP-bound state), 10 mM $MgSO_4$ (Ver/MgATP state) and 0.25 mM Vi (Ver/Vi state). The two dominant exponential components of the sensitized emission decays are presented as distances d1 and d2. Lifetimes of Bodipy FL-sensitized emission (τ_{DA}), the calculated donor-acceptor distances (R) and the percentage of NT Pgp molecules displaying each distance are shown. The latter were calculated from multi-exponential fits as the fractional intensity contribution of each exponential component divided by the rate of energy transfer ($k = 1/\tau_{DA} - 1/\tau_D$). Data are presented as means \pm SEM, and n is the number of independent experiments. All the LRET decays used for these calculations were obtained from NT Pgp in NDSCs at 37°C.

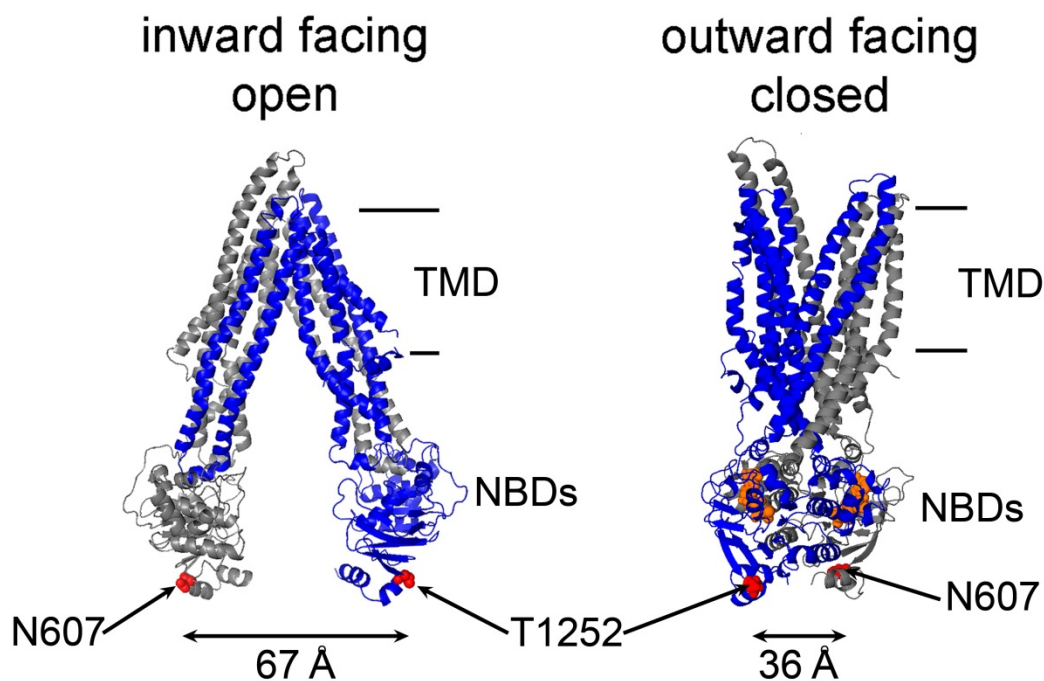


FIGURE 1. Alternating access model of Pgp with large NBD-NBD separation in the apo state. Binding of ATP to the NBDs promotes the transition from the nucleotide-free inward-facing conformation (apo; PDB: 4Q9H) to the outward-facing conformation (nucleotide-bound model (47) based on the X-ray crystal structure of nucleotide-bound Sav1866; PDB: 2ONG). The first and second homologous halves are represented in gray and blue, respectively. In this study, N607 and T1252 (red spheres) were mutated to Cys to chemically attach LRET probes. The approximate position of the membrane is between the lines on the right. TMD: transmembrane domain; NBDs: nucleotide-binding domains.

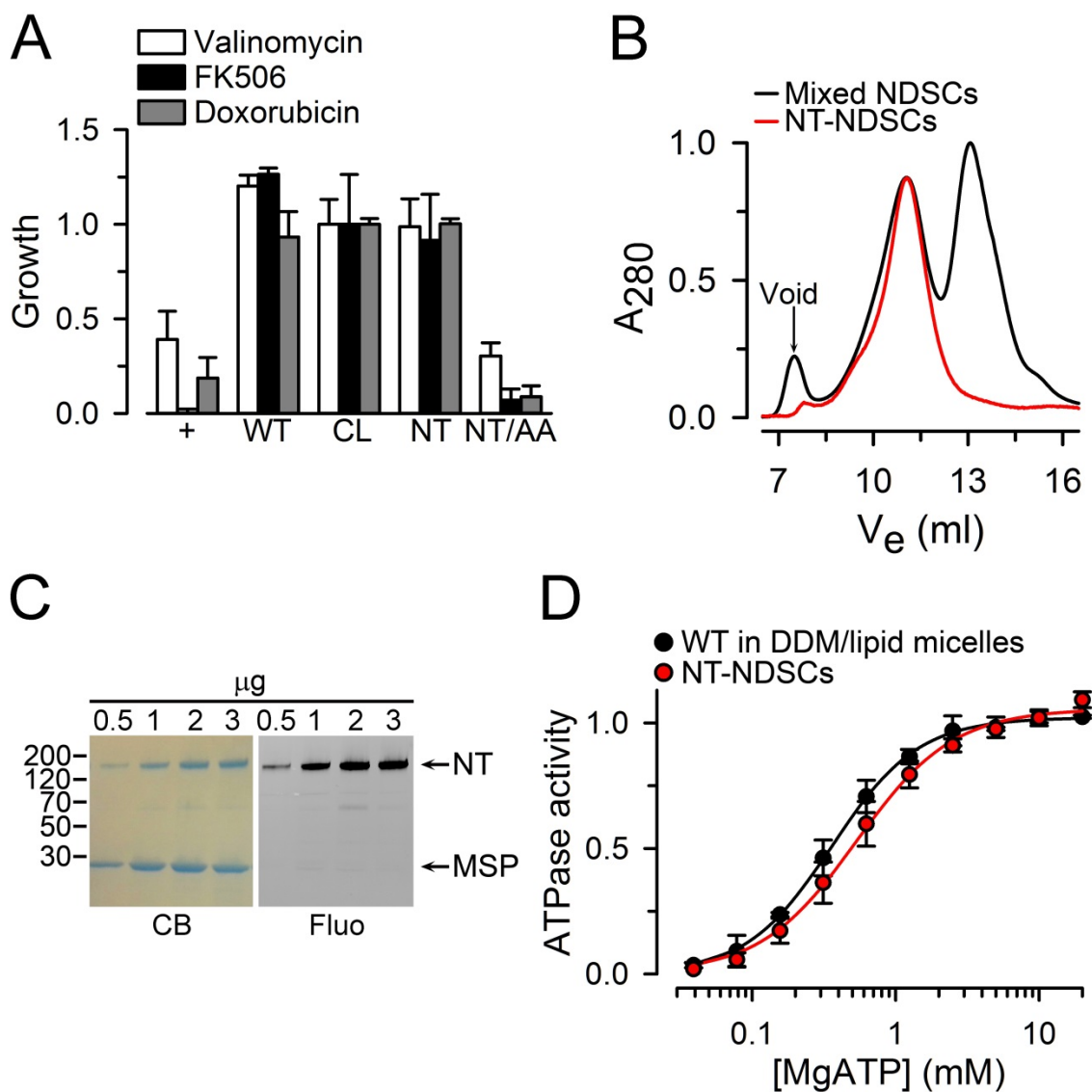


FIGURE 2. Characterization of NT Pgp. *A*, Drug resistance assay in *S. cerevisiae*. The relative growth of cells transformed with the pVT vector control (-), and cells expressing wild-type Pgp (WT), Cys-less Pgp (CL), the N607C/T1252C (NT) or E552A/E1197A (NT/AA) mutants was monitored in the presence of 100 μ M valinomycin, 62 μ M FK506 or 40 μ M doxorubicin for 25-30 h at 28°C. Data were normalized to the CL Pgp average and are presented as means \pm SD of 3 independent experiments performed in duplicate. *B*, Size-exclusion chromatography elution profile of NT Pgp purified and reconstituted in lipid nanodiscs (NDSCs). The two main peaks of the black trace correspond to NDSCs containing Pgp (V_e ~11 ml) and empty NDSCs (V_e ~13 ml). The red trace corresponds to NT Pgp in NDSCs (NT-NDSCs) purified by affinity chromatography (anti-FLAG M2 affinity gel) from the mixed NDSCs. *C*, NT Pgp in NDSCs. Coomassie stained PAGE-SDS gel (CB) and the corresponding fluorescent image (Fluo) of the fraction enriched in NDSCs containing NT Pgp labeled with Bodipy FL. Arrows point to the NT Pgp (NT) and MSP bands. Molecular masses of selected markers, in kDa, are shown on the left. *D*, ATPase activity measured in the presence of 30 μ M verapamil. Data are averages \pm SEM of at least 3 independent experiments. Lines represent fits to the Hill equation, with Hills coefficients of 2 and 1.8 for WT Pgp and NT Pgp, respectively. V_{max} and K_m values were not significantly different between WT Pgp (V_{max} = 3.9 \pm 0.4 μ mol/min/mg; K_m = 0.31 \pm 0.03 mM) and NT Pgp (V_{max} = 4.1 \pm 0.5 μ mol/min/mg; K_m = 0.27 \pm 0.02 mM).

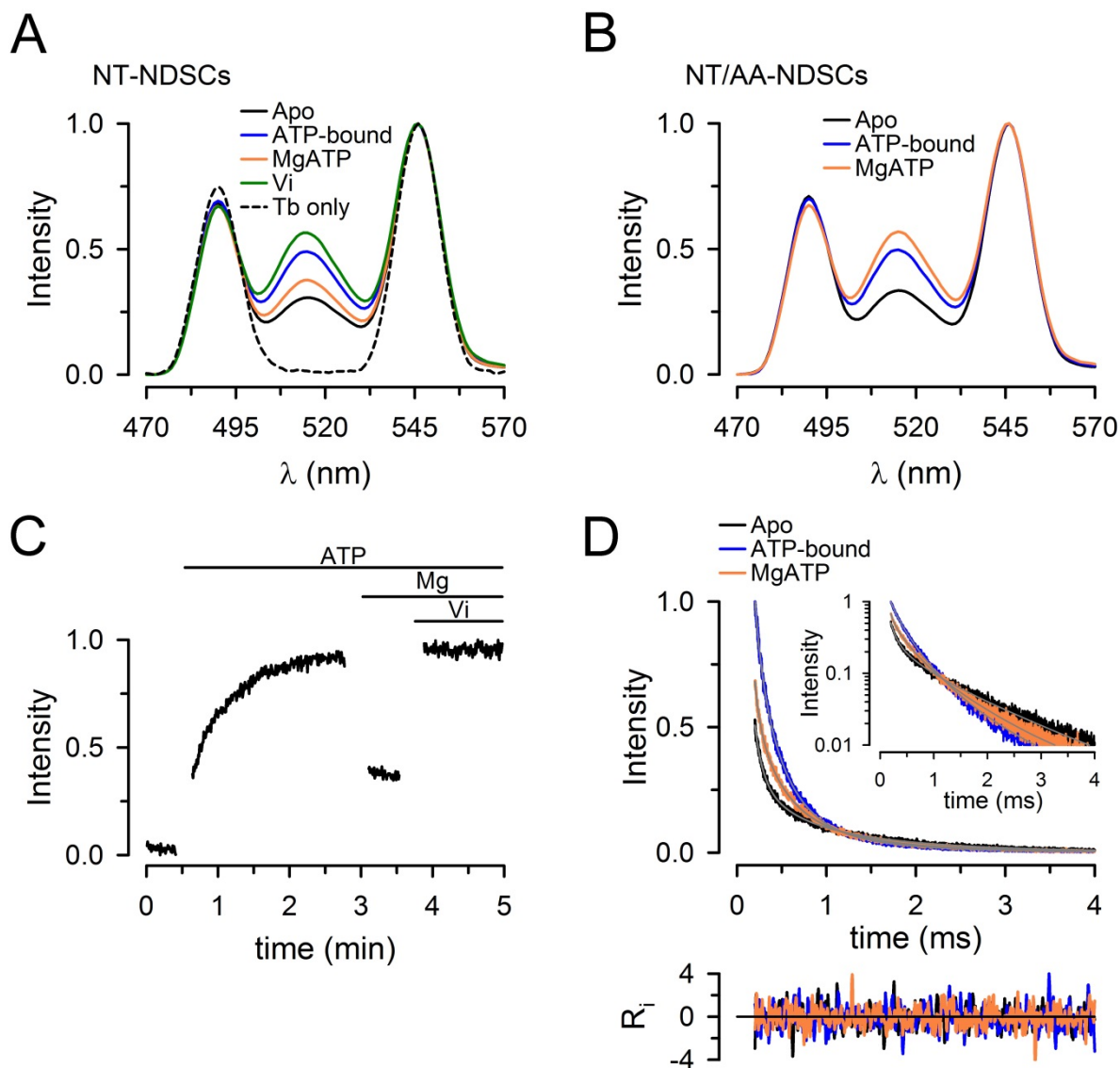


FIGURE 3. Conformational changes during the ATP hydrolysis cycle of NT Pgp in NDSCs at 37°C. *A*, Emission spectra from NDSCs containing NT Pgp labeled with donor only (Tb^{3+} chelate) or donor and acceptor (Tb^{3+} chelate and Bodipy FL). Traces were normalized to the Tb^{3+} emission at 546 nm. *B*, Emission spectra of the catalytically-inactive mutant NT/AA Pgp in NDSCs. *C*, Time course of the changes in Bodipy FL sensitized emission, recorded at 520 nm, in response to sequential additions of NaATP, $MgSO_4$ and Vi. The gaps during the recording correspond to time periods where additions and manual mixing were performed. The intensity was normalized to the maximum obtained after addition of Vi. *D*, Bodipy FL sensitized emission decays, recorded at 520 nm, from NT Pgp in NDSCs. The inset displays the same curves in a semi-log scale. R_i represents the weighted residuals of the multi-exponential fits (gray lines in the main graph and inset). Decays were normalized to the emission of the ATP-bound protein at 200 μs . All the traces in the figures are representative of at least 7 independent experiments and were obtained at 37°C. Apo: nucleotide- and drug-free buffer with 1 mM EDTA; ATP-bound: + 5 mM NaATP; MgATP: + 10 mM $MgSO_4$.

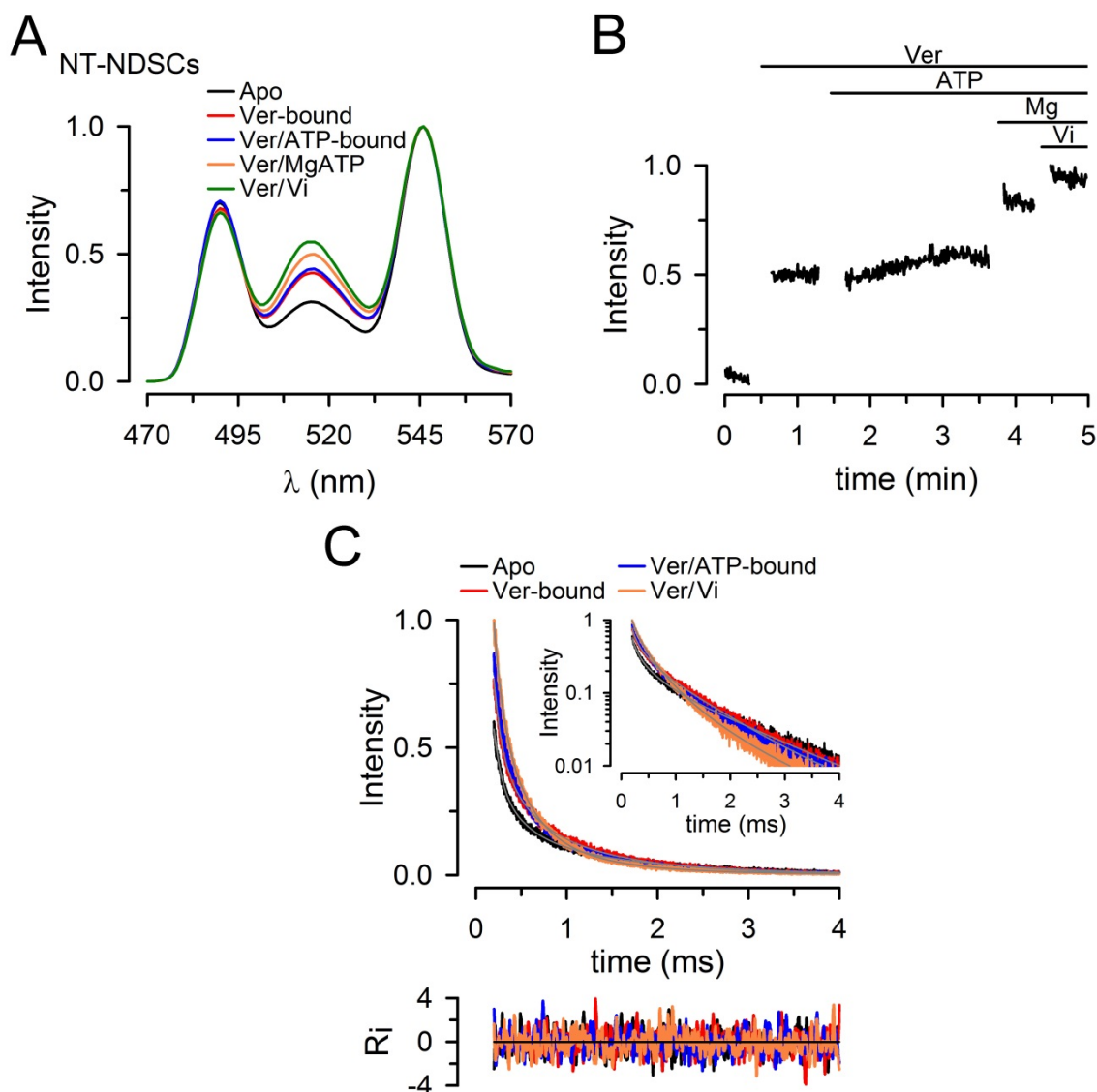


FIGURE 4. Conformational changes during the ATP hydrolysis cycle of NT Pgp in NDSCs at 37°C in the presence of verapamil. *A*, Emission spectra from NDSCs containing NT Pgp labeled with donor (Tb^{3+} chelate) and acceptor (Tb^{3+} chelate and Bodipy FL). *B*, Time course of the changes in Bodipy FL sensitized emission in response to sequential additions of Ver, NaATP, MgSO_4 and Vi. Intensity was normalized to the maximum obtained after addition of Vi. *C*, Bodipy FL sensitized emission decays, recorded at 520 nm, from NT Pgp in NDSCs. Decays were normalized to the emission of the Ver/Vi state at 200 μs . All the traces shown in these figures are representative of at least 5 independent experiments and were obtained at 37°C. Apo: nucleotide- and drug-free buffer with 1 mM EDTA; Ver: + 30 μM verapamil; Ver/ATP-bound: + 5 mM NaATP; Ver/MgATP: + 10 mM MgSO_4 ; Ver/Vi: + 0.25 mM Vi. See legend to Fig. 3 for details.

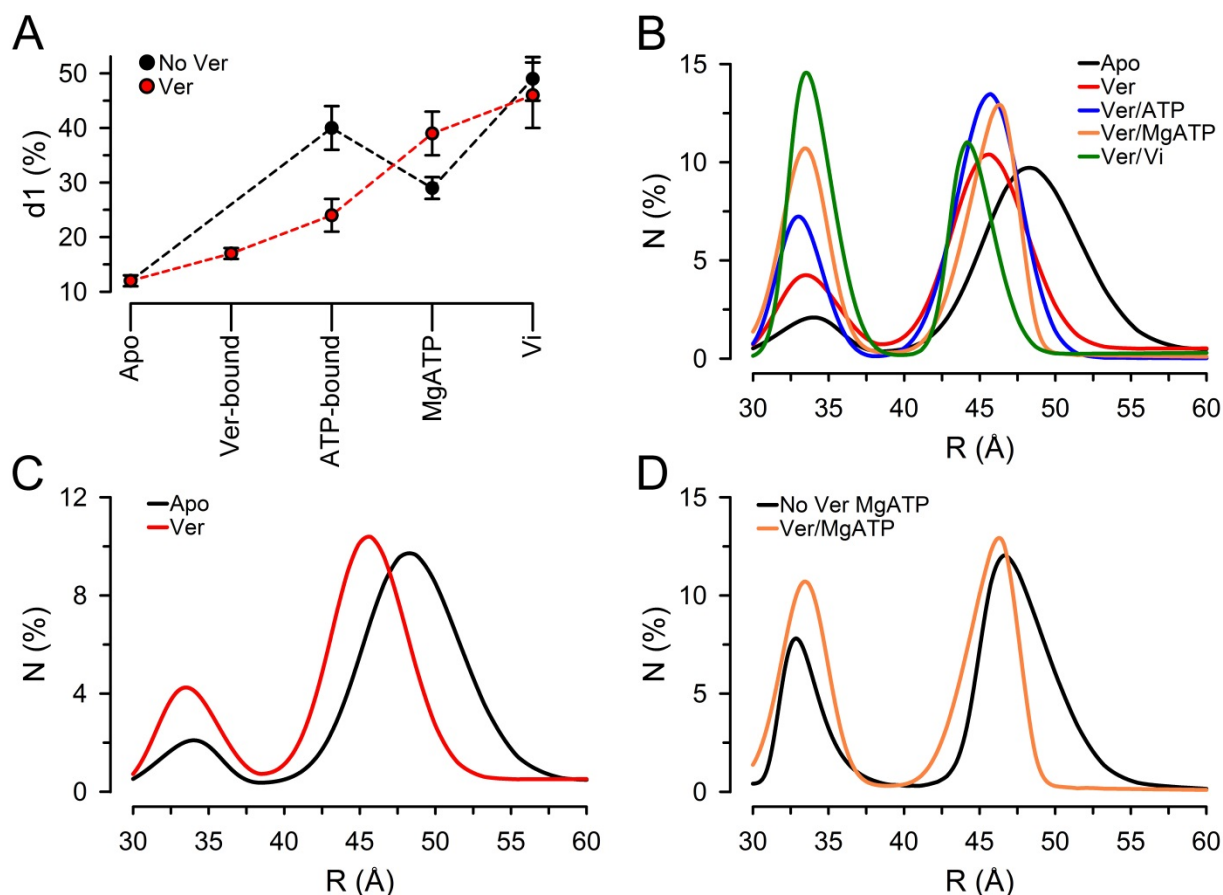


FIGURE 5. Distance distributions of NT Pgp in NDSCs at 37°C in different states during the hydrolysis cycle. *A*, Percentage of NT Pgp molecules displaying the shorter distance (d_1 , ~33 Å). Means \pm SEM in the absence (No Ver; $n = 7$) and presence of Ver ($n = 5$) were calculated from the multi-exponential fits results (Table 1) as the fractional intensity contribution of each exponential component divided by the rate of energy transfer ($k = 1/\tau_{DA} - 1/\tau_D$). *B*, Distance distributions calculated from LRET sensitized emission intensity decays analyzed by an exponential series method. N : % molecules. The percentage of molecules in each conformation, calculated as described in the legend to panel *A*, was adjusted based on the cumulative number of molecules *vs.* donor-acceptor pair distance obtained from the exponential series method analysis. See Materials and methods and Supplementary Fig. 8 for details. Solid lines correspond to the best fits obtained using Peak Fit (Systat Software Inc., San Jose, CA). Apo: nucleotide- and drug-free buffer with 1 mM EDTA; Ver: + 30 μ M Ver; Ver/ATP-bound: + 5 mM NaATP; Ver/MgATP: + 10 mM $MgSO_4$; Ver/Vi: + 0.25 mM Vi. *C*, Comparison of distance distributions in the apo state (No Ver) and in the presence of Ver (Ver). *D*, Comparison of distance distribution during hydrolysis in the absence (MgATP) and presence of Ver (Ver/MgATP). Data from NT Pgp in NDSCs at 37°C were used for all calculations. The curves in panels *B-D* are averages from 5 independent experiments.

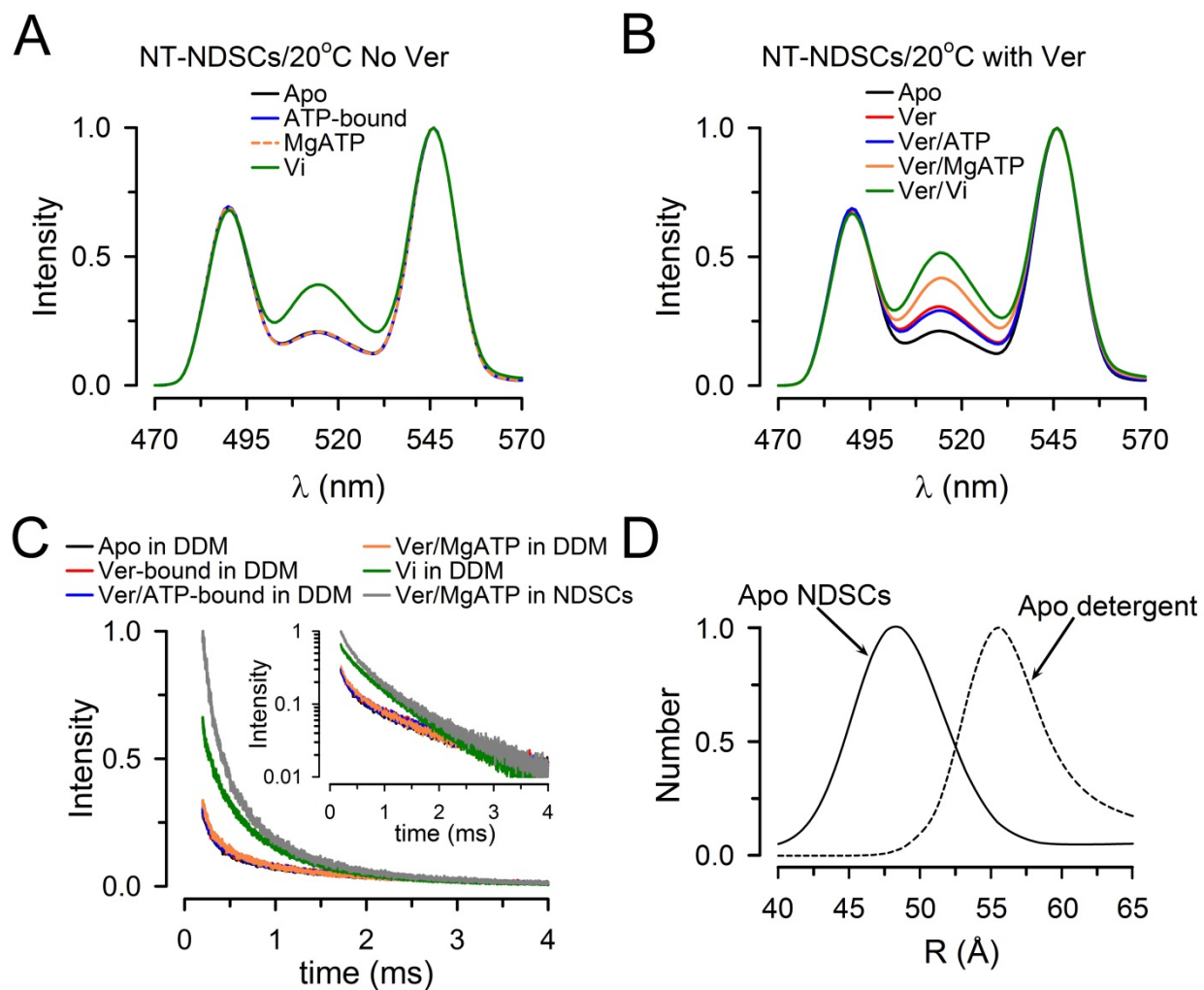
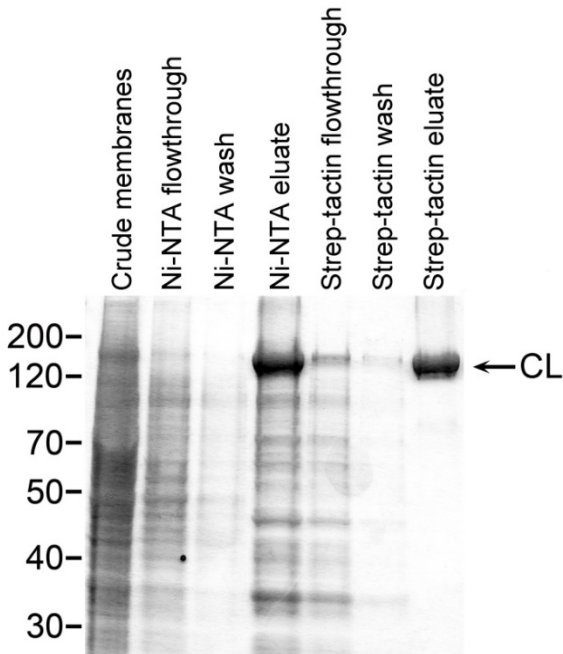


FIGURE 6. Conformational changes during the ATP hydrolysis cycle of NT Pgp in NDSCs at 20°C. *A*, Emission spectra from NDSCs containing NT Pgp measured in the absence of Ver. Apo: nucleotide- and drug-free buffer with 1 mM EDTA; ATP-bound: + 5 mM NaATP; MgATP: + 10 mM MgSO₄; Vi: + 0.25 mM Vi. *B*, Emission spectra from NDSCs containing NT Pgp measured in the presence of Ver. Apo: nucleotide- and drug-free buffer with 1 mM EDTA; Ver: + 30 μM Ver; Ver/ATP-bound: + 5 mM NaATP; Ver/MgATP: + 10 mM MgSO₄; Ver/Vi: + 0.25 mM Vi. *C*, Bodipy FL sensitized emission decays from NT Pgp in detergent (DDM; 0.1% n-dodecyl-β-D-maltopyranoside) or NDSCs. The inset displays the same curves in a semi-log scale. Decays were normalized to the emission at 200 μs of NT Pgp in NDSCs in the Ver/MgATP state. *D*, Distribution of Pgp molecules displaying the d2 distance (longer distance) determined at 20°C in the apo state of NT Pgp in DDM and in NDSCs. The y-axis represents the relative number of molecules displaying the d2 distance. All the traces shown in these figures are representative of at least 3 independent experiments and were obtained at 20°C. Emission was recorded after a 200 μs delay from the 337-nm excitation pulse. See legend to Fig. 3 for details.

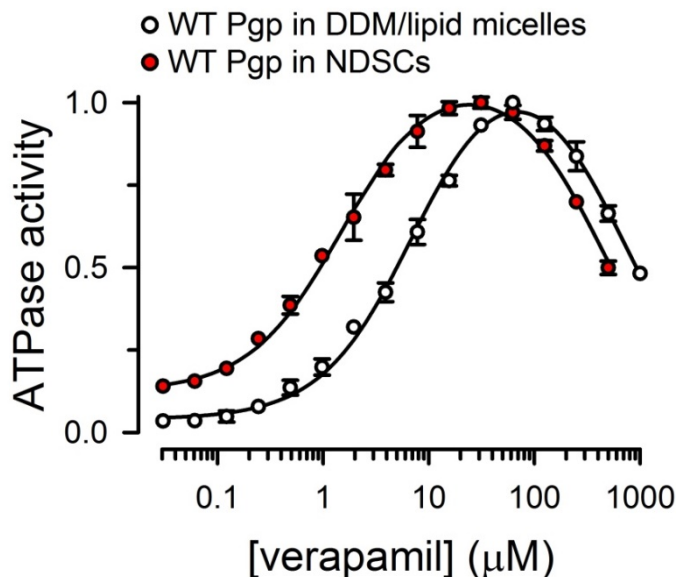
Supplementary Information

Substrate-induced conformational changes in the nucleotide-binding domains of lipid bilayer-associated P-glycoprotein during ATP hydrolysis

Maria E. Zoghbi^{#1}, Leo Mok^{#2}, Douglas J. Swartz², Anukriti Singh², Gregory A. Fendley¹, Ina L. Urbatsch^{2,3} and Guillermo A. Altenberg^{1,3}



Supplementary Fig. 1. **Example of Pgp purification.** Samples were subjected to SDS-PAGE and the gel was stained with Coomassie blue. The example corresponds to the purification of Cys-less Pgp (CL), but the results were essentially identical for WT Pgp, NT Pgp and NT/AA Pgp. Molecular masses of selected markers, in kDa, are shown on the left. See main text for details.

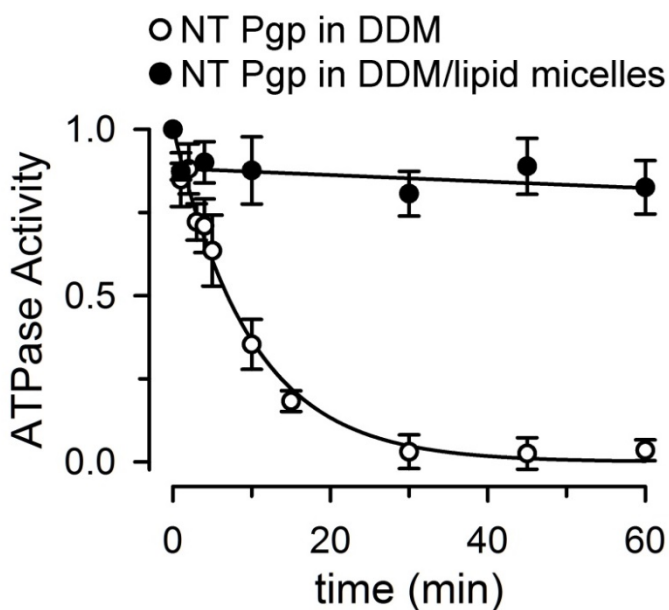


Supplementary Fig. 2. **Verapamil (Ver)-stimulated ATPase activity of WT Pgp.** WT Pgp activity was assayed at 37°C in the presence of 10 mM ATP and 12 mM MgSO₄ in 0.1% DDM supplemented with 0.6% (w/v) *E. coli* lipids (WT Pgp in DDM/lipid micelles) and in NDSCs. Data are means ± SD (n = 3 for each condition). SDs smaller than the symbols are not shown). Activities were normalized to maximal measured rates (5.0 ± 0.1 μmol/min/mg for Pgp for detergent/lipid micelles and 5.2 ± 0.1 μmol/min/mg for Pgp in NDSCs). Lines represent fits to the equation:

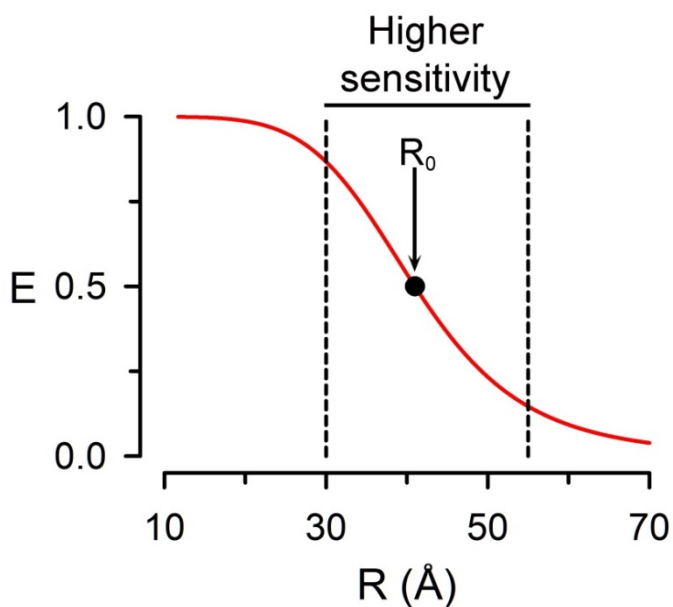
$$V = V_b + ((V_{max} - V_b) \cdot Ver / (K_S + Ver)) \cdot (1 - (V_{max} - V_F) / (V_{max} - V_b) \cdot (Ver / K_I + Ver))$$

V: rate of ATP hydrolysis; V_b: basal

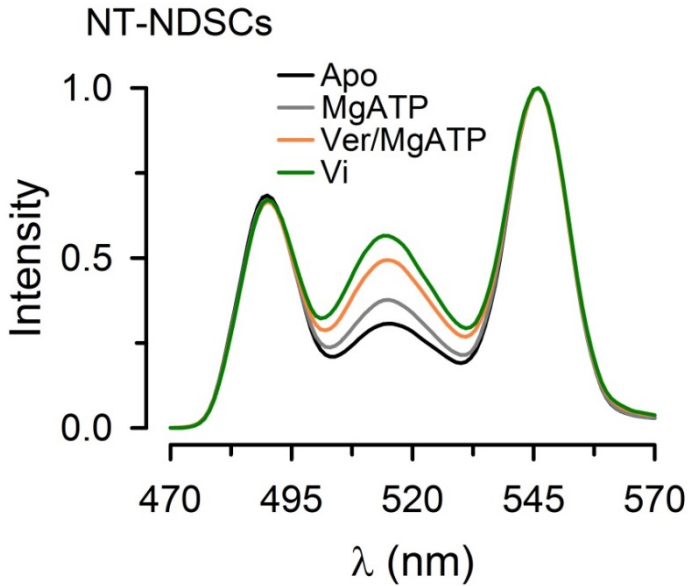
ATPase activity; V_{max}: maximal ATPase activity; Ver: verapamil concentration; K_S: EC₅₀ for the stimulatory effect; V_F: ATPase activity at ∞ Ver; K_I: IC₅₀ for the inhibitory effect. The average K_S values for Pgp in NDSCs and micelles were 1.5 and 7.3 μM, respectively.



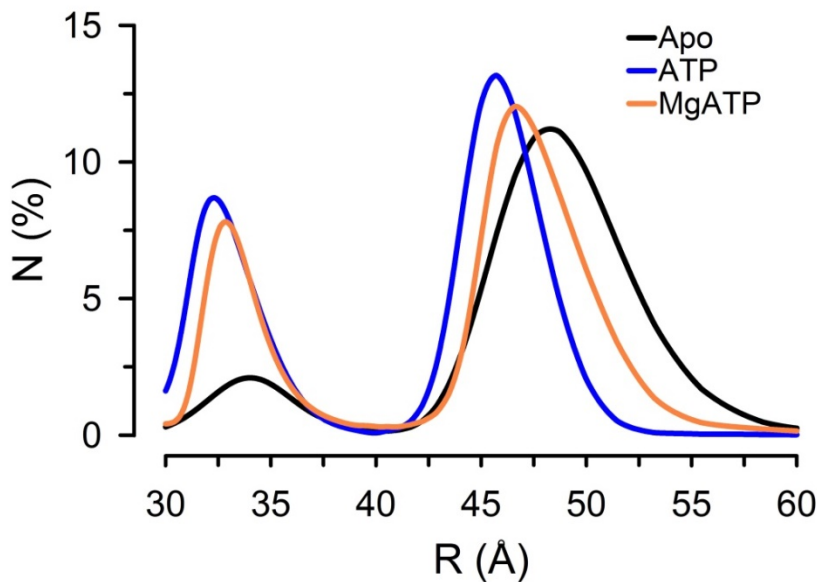
Supplementary Fig. 3. **Stability of the Pgp-NT ATPase.** Activities of Pgp NT in 0.1% n-dodecyl- β -D-maltopyranoside (DDM) in the absence of lipids (Pgp-NT in DDM) and after supplementation with 0.6% (w/v) *E. coli* lipids (Pgp-NT in DDM/lipid micelles). The ATPase activity was measured at 37°C and data are means \pm SD (n = 3 for each condition).



Supplementary Fig. 4. **Dependence of energy transfer (E) on Tb³⁺-Bodipy FL distance.** The curve was generated from: $R = R_0 (E^{-1} - 1)^{1/6}$, where R is the donor-acceptor distance and R₀ is the Förster distance (the distance at which E = 0.5). The R₀ determined for the Tb³⁺/Bodipy Fl pair was 41 Å.

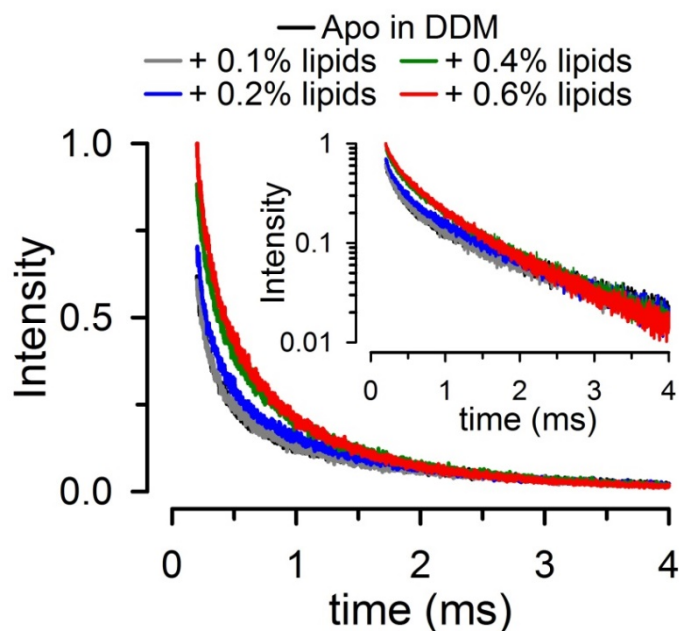


Supplementary Fig. 5. **Increase in sensitized Bodipy FL emission during hydrolysis by addition of verapamil.** Emission spectra from NDSCs containing Pgp NT labeled with donor (Tb^{3+} chelate) and acceptor (Bodipy FL). Traces obtained sequentially at $37^{\circ}C$ were normalized to the Tb^{3+} emission at 546 nm and are representative of at least 3 independent experiments. Emission was recorded after a 200 μs delay from the 337-nm excitation pulse. Apo: nucleotide- and drug-free buffer with 1 mM EDTA; MgATP: + 5 mM MgATP; Ver/MgATP: + 30 μM verapamil; Ver/Vi: + 0.25 mM Vi.

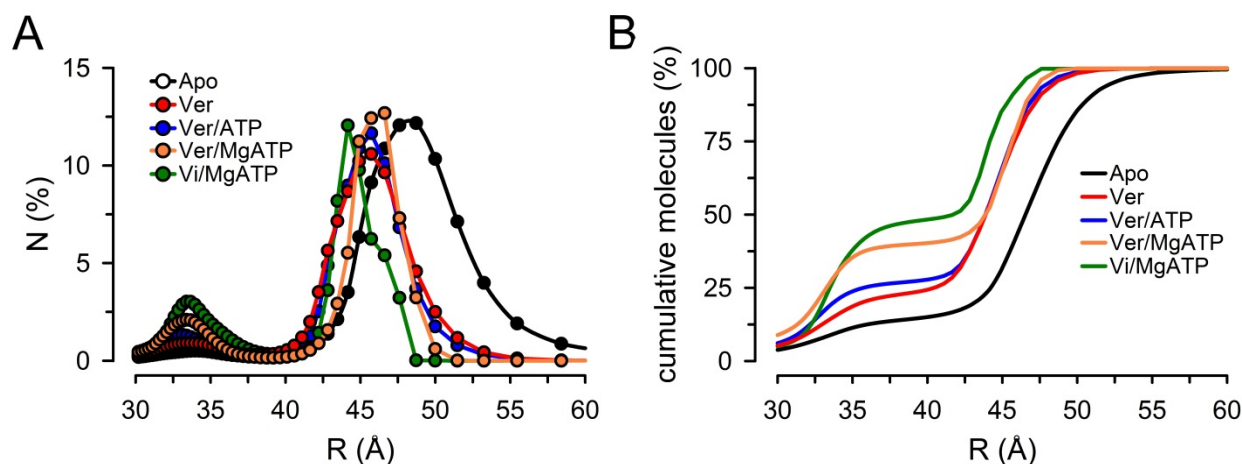


Supplementary Fig. 6. **Distance distributions of Pgp NT in NDSCs in the absence of transport substrate.** Distance distributions calculated from LRET sensitized emission intensity decays analyzed by an exponential series method. N: % molecules. The percentage of molecules in each conformation was adjusted based on the cumulative number of molecules vs. donor-acceptor pair distance obtained from the exponential series method analysis. See Experimental Procedures and Supplementary Fig. 8 for details. Data correspond to the best fits

obtained using Peak Fit (Systat Software Inc., San Jose, CA) using data from 7 independent experiments. Apo: nucleotide- and drug-free buffer with 1 mM EDTA; ATP: + 5 mM NaATP; MgATP: + 10 mM $MgSO_4$. Data from Pgp-NT in NDs at $37^{\circ}C$ were used for all calculations.



Supplementary Fig. 7. **Conformational changes elicited by addition of lipids to Pgp NT in detergent in the apo state.** Bodipy FL sensitized emission decays, recorded at 520 nm, from Pgp NT in detergent (DDM; 0.1% n-dodecyl- β -D-maltopyranoside) before and after addition of *E. coli* lipids (in %; w/v) to produce mixed DDM/lipid micelles. Pgp NT was studied in the apo state (nucleotide- and drug-free buffer with 1 mM EDTA). The inset displays the same curves in a semi-log scale. Decays were normalized to the emission measured in the presence of 0.6% lipids at 200 μ s. Traces are representative of at least 3 independent experiments and were obtained at 20°C. Emission was recorded after a 200 μ s delay from the 337-nm excitation pulse.



Supplementary Fig. 8. **Distance distributions of Pgp NT in NDSCs under different states during the hydrolysis cycle.** **A**, Distance distributions calculated from LRET sensitized emission intensity decays analyzed by an exponential series method. N: % molecules. The symbols denote the calculated average values and are joined by spline lines. **B**, Cumulative number of molecules vs. donor-acceptor pair distance. Data were obtained by cumulative addition of N determined by the exponential series method analysis (panel A). The percentage of molecules in each conformation in Fig. 5 of the accompanying manuscript was calculated from the fractional intensity contribution of each exponential component divided by the rate of energy transfer ($k = 1/\tau_{DA} - 1/\tau_D$), and was adjusted based on the cumulative number of molecules vs. donor-acceptor pair distance obtained from the exponential series method analysis (panel B). Apo: nucleotide- and drug-free buffer with 1 mM EDTA; Ver: + 30 μ M verapamil; Ver/ATP-bound: + 5 mM NaATP; Ver/MgATP: + 10 mM MgSO₄; Ver/Vi: + 0.25 mM Vi. Data from Pgp NT in NDs at 37°C were used for all calculations (n = 5). See Experimental Procedures for references and additional details.

Substrate-induced conformational changes in the nucleotide-binding domains of lipid bilayer-associated P-glycoprotein during ATP hydrolysis

Maria E. Zoghbi, Leo Mok, Douglas J. Swartz, Anukriti Singh, Gregory A. Fendley, Ina L. Urbatsch and Guillermo A. Altenberg

J. Biol. Chem. published online October 9, 2017 originally published online October 9, 2017

Access the most updated version of this article at doi: [10.1074/jbc.M117.814186](https://doi.org/10.1074/jbc.M117.814186)

Alerts:

- [When this article is cited](#)
- [When a correction for this article is posted](#)

[Click here](#) to choose from all of JBC's e-mail alerts

Supplemental material:

<http://www.jbc.org/content/suppl/2017/10/09/M117.814186.DC1>